Tailoring the structure of casein micelles through a multifactorial approach to manipulate rennet coagulation properties

Fanny Lazzaro[1,2*], Antoine Bouchoux[3], Jared Raynes[4], Roderick Williams[4], Lydia Ong[5,6,7], Eric Hanssen[6], Valérie Lechevalier[1], Stéphane Pezennec[1], Hyun-Jung Cho[8], Amy Logan[4], Sally Gras[5,6,7], Frederic Gaucheron[1]

[1] STLO, Agrocampus Ouest, INRA, 35000, Rennes, France

[2] CNIEL, Paris, France

[3] LISBP, Université de Toulouse, CNRS, INRA, INSA, Toulouse, France

[4] CSIRO Agriculture & Food, 671 Sneydes Road, Werribee, Victoria 3030, Australia

[5] Department of Chemical Engineering, The University of Melbourne, Parkville, Victoria 3010, Australia

[6] Advance Microscopy Facility, The Bio21 Molecular Science and Biotechnology Institute, The University of Melbourne, Parkville, Victoria 3010, Australia

[7] The ARC Dairy Innovation Hub, The University of Melbourne, Parkville, Victoria, 3110

[8] Biological Optical Microscopy Platform, University of Melbourne, Parkville VIC 3010, Australia

* Corresponding author. STLO, Agrocampus Ouest, INRA, 65 rue de Saint-Brieuc 35000, Rennes, France. flazzaro@hotmail.fr

Abstract:

The internal structure of the casein micelle remains a matter of debate. The two latest models published consider the presence of at least three levels of structure: the casein micelle; dense regions within the micellar structure, and calcium phosphate nanoclusters and/or proteins inhomogeneities. The properties of casein micelles are affected by modifications to the environment, such as variations in pH or the addition of salts: The scientific literature typically considers the effects of one factor at a time, while in industrial processes, several modifications are performed simultaneously.

The aim of this study was to assess the impact of multifactorial environmental modifications on the colloidal, structural and rennet coagulation properties of casein micelles. The experimental design involved variations in pH, together with the addition of NaCl and $CaCl_2$.

A key finding was that dense regions (~ 20 nm in size) could be released from the casein micelle. The addition of NaCl and $CaCl_2$ had opposing effects, *i.e.* enhancing or limiting this micellar disruption, respectively. A decrease in pH had the strongest impact on the mineral balance, causing the colloidal CaP to solubilize and the micelle to swell. The rennet clotting time was impacted by variations in pH and NaCl content. Interestingly, a consideration of all three levels of casein micelle structure and their interactions was needed to explain variations in the firmness of rennet gels. This study illustrates the complex interplay of factors affecting micellar structure and improves our understanding of how micelles can be manipulated to control their properties.

Keywords: casein micelle, rennet properties, internal structure, multifactorial modifications, small angle neutron scattering, cryo transmission electron microscopy

1 Introduction

In milk, casein proteins (α_{s1}, α_{s2}, β and κ) and minerals (mainly calcium phosphate (CaP) nanoclusters) self-assemble to form a colloid referred to as the casein micelle. Electrostatic, hydrophobic and Van der Waals forces hold the different components together leading to a polydisperse population of particles 100 – 200 nm in diameter (Dalgleish & Corredig, 2012; Holt, Carver, Ecroyd, & Thorn, 2013; Holt, 2016; Holt & Horne, 1996; Horne, 2017; Thorn et al., 2005).There is a consensus that casein micelles are stabilized through electrostatic and steric repulsions due to the presence of a polyelectrolyte brush of κ-casein at the micellar surface (de Kruif, 1999; de Kruif & Zhulina, 1996; Tuinier & de Kruif, 2002). Despite extensive studies the internal structure of the casein micelle, *i.e.* the interactions between caseins and the minerals located within the colloid structure, is still under debate. The recent use of small angle X-ray and neutron scattering (SAXS and SANS, respectively) in parallel with cryo-transmission electron microscopy (cryo-TEM) has enabled questions around the internal structure to be partially answered, although without general agreement (Bouchoux et al., 2015; Bouchoux, Gésan-Guiziou, Pérez, & Cabane, 2010; Day, Raynes, Leis, Liu, & Williams, 2017; De Kruif, 2014; Ingham et al., 2015, 2016; Marchin, Putaux, Pignon, & Léonil, 2007; Pignon et al., 2004; Shukla, Narayanan, & Zanchi, 2009). To date, the previously most accepted submicelle model (Schmidt, 1982; Walstra, 1999) has been progressively abandoned in favor of a more open structure composed of dense regions, water channels and CaP nanoclusters.

Environmental factors such as variations in pH, temperature and the addition of salts or chelating agents (de Kort, Minor, Snoeren, van Hooijdonk, & van der Linden, 2011; Gaucheron, 2004; Lazzaro et al., 2017; Silva et al., 2013) induce shifts in the mineral balance between the diffusible and colloidal phases of the casein micelle. These mineral modifications also involve colloidal modifications that lead to changes in the functional properties of the casein micelle, such as the formation and stability of emulsions, thermal stability, and response to acid and rennet coagulation (Broyard & Gaucheron, 2015; Gaucheron, 2004). Although the mineral

fraction only represents a small proportion of the milk components (0.7%), it is used to control the properties of numerous manufactured dairy products.

This study focuses on the gelation of the casein micelle following the addition of chymosin (rennet), which forms the first step of cheese manufacture. The rennet coagulation mechanism can be divided into three steps: firstly, chymosin hydrolyzes the κ-casein of the casein micelle by cleaving the Phe(105)-Met(106) bond. Next, once a sufficient amount of κ-casein is hydrolyzed the depleted casein micelles aggregate (Lucey, 2002) and finally, this aggregation is followed a reorganization and reticulation of the casein gel (Dalgleish & Corredig, 2012).

Rennet coagulation can be assessed by two main characteristics: (i) the rennet clotting time (RCT), the time elapsed from the addition of rennet or chymosin to the detectable onset of gelation and (ii) the firmness of the gel. The RCT mainly depends on the rate of the enzymatic reaction and the aggregation of the paracaseinates (first and second steps), while the firmness depends on the organization and the strength of the gel (third step).

Variations in pH and the addition of NaCl and $CaCl_2$ are steps commonly applied in cheese manufacture to control the coagulation of milk. Many studies have been published describing the separate influence of each of these parameters on the colloidal properties and on the rennet coagulation properties of the casein micelle e.g.:(Bulca, Wolfschoon-Pombo, & Kulozik, 2016; Choi, Horne, & Lucey, 2007; Daviau, Famelart, Pierre, Goudedranche, & Maubois, 2000; Deeth & Lewis, 2015; Famelart, Le Graet, & Raulot, 1999; Famelart, Lepesant, Gaucheron, Le Graet, & Schuck, 1996; Grufferty & Fox, 1985; Karlsson, Ipsen, & Ardö, 2007; Karlsson et al., 2007; Sandra, Ho, Alexander, & Corredig, 2012; Sbodio, Tercero, Coutaz, & Revelli, 2006; Zhao & Corredig, 2015; Zoon, van Vliet, & Walstra, 1988, 1989). Although necessary to understand the dissociated effect of each parameter, this monofactorial approach does not correspond to the reality of the cheese industry where a multifactorial approach occurs with the simultaneous variation of several parameters.

The aim of the current study was to investigate the effect of simultaneous modification of the physico-chemical parameters on both the colloidal properties and the rennet induced coagulation casein micelles. An experimental matrix of 27 different suspensions of casein micelles in water, with variations in added NaCl and $CaCl_2$, at three different pH was designed. A combination of multiple advanced biophysical techniques, such as cryo-TEM and SAXS, was used to make a thorough characterization of the casein micelles in terms of physicochemical, structural and renneting properties. Appropriate statistical analyses were applied to establish the relationships between the colloidal and the rennet coagulation properties of the modified casein micelles, leading to the first study that combines SAXS characterization with an assessment of the functional properties of casein micelles.

2 Materials and methods

2.1 Chemicals

All chemicals used for this study, hydrochloric acid (VWR chemicals, Fontenay-sous-bois, France), NaCl (PanReac AppliChem, Barcelona, Spain), $CaCl_2$ (VWR International, Leuven, Belgium) and sodium azide (Riedek-de Haën, Seelze, Germany) were of analytical grade.

2.2 Materials

Experiments were carried out using a native phosphocaseinate (NPC) powder resuspended in deionised water at 24.2± 0.8 g kg^{-1} of protein. Concentrated NPC was supplied by Gillot SAS (Saint Hilaire de Briouze, France) and obtained by microfiltration (0.1 µm pore size membrane) of raw skimmed milk followed by diafiltration against milli-Q water. The concentrate was then spray dried according to the method described by Pierre, Fauquant, Le Graet, & Maubois (1992) and Schuck et al., (1994) using Bionov facilities (Rennes, France). Casein and their associated minerals represented more than 90% of the total solid content of the powder. Residual whey proteins (3%) (w/w) and traces of lactose were present in the powder.

For the coagulation experiments, Chr. Hansen (Hoersholm, Denmark) supplied commercial chymosin (CHY-MAX M 200, 200 IMCU ml^{-1}).

2.3 Preparation of casein micelle suspensions

An experimental matrix was designed to assess the concomitant effects of variations in pH and the addition of NaCl or $CaCl_2$. The range of pH and the final concentrations of added NaCl and $CaCl_2$ were selected to produce suspensions which would form gels within one hour after the addition of a set amount of chymosin. The pH values targeted were 5.7, 6.3 or 6.9 and the final concentrations of NaCl and $CaCl_2$ in the suspensions were 0, 50 and 100 mmol kg^{-1} or 0, 7.5 and 15 mmol kg^{-1}, respectively. A full experimental design was carried out, where 27 different suspensions of casein micelles were prepared in water, with different salt and pH environments. The suspensions were named from A to Z, and CTRL to represent the control which consisted of NPC in water at pH 6.9, with no added salts (Fig.1).

Dispersion of the NPC powder in milli-Q water was performed as described in Lazzaro et al., (2017). Varying amounts of stock solutions of NaCl (2.5 mol kg^{-1} in milli-Q water, pH 6.9) and $CaCl_2$ (0.25 mol kg^{-1} in milli-Q water, pH 6.9) were added to the concentrated suspensions of NPC in milli-Q water, in such a way that after the dilution step (see below), the required concentrations in salts were reached (Fig.1). The suspensions were stirred for 30 min. The pH shift induced by the addition of salts was corrected using HCl 1M in milli-Q water and set to 5.7, 6.3 or 6.9 (Fig.1). The suspensions were then diluted to 24.2 ± 0.8 g kg^{-1} of protein and left overnight at room temperature. If necessary, the pH was readjusted prior to experiments. For convenience, Tables 1, 2, 3 and Figures 6, 7, 8 report the results of different analyses on a set on 9 samples only. These selected samples correspond to the corners of the cubic experimental design (suspensions A, B, D, E, J, L, M, CTRL ; extreme points) and the center point of the experimental design (suspension T) (Fig. 1).

2.4 Recovery of the diffusible phases of the suspensions

Aliquots (15mL) of each NPC suspension were ultrafiltered by centrifugation for 30 min, at 20°C and 1800 *g*. using Vivaspin concentrators (molecular weight cut-off 10 kD, Vivascience, Palaiseau, France). The diffusible phases were analyzed to determine the concentrations of diffusible ions and used for the dilution of the suspension for the turbidity (τ) and nanoparticle tracking analysis (NTA) measurements and for the background determination for the SAXS measurements.

2.5 Analysis

2.5.1 Protein content

The total nitrogen content of each suspension was determined according to the Kjeldahl method (IDF standard 20-1, 2014). A factor of 6.38 was used to convert nitrogen to protein concentration. Measurements were performed in duplicate.

2.5.2 Mineral composition and distribution

Total and diffusible cations (calcium Ca, sodium Na) and anions (chloride Cl, inorganic phosphate Pi) contents were determined as described in (Lazzaro et al., 2017). Colloidal concentrations were deduced by subtracting the concentration of diffusible ions from the concentration of total ions. The mineral concentrations were adjusted to account for the small differences in protein content (see section 2.5.1.)

2.5.3 Turbidity measurements

Absorbance measurements were carried out at 600 nm and 20 °C using a UV-visible spectrometer (UVmc², Safas, Monaco).The casein micelle suspensions were diluted 10 times in their diffusible phases and analyzed immediately. The diffusible phase for each suspensions was also analyzed. Absorbance measurements were converted into turbidity (τ) according to the following formula:

$$\tau = 2.303 * \frac{OD(600nm)}{l}$$

with $OD(600nm)$ being the optical density of the suspension (difference between the absorbance of the diluted suspension and the absorbance of its diffusible phase) ; and l the light path length ($l = 1\,cm$).

2.5.4 Nanoparticle tracking analysis

Nanoparticle Tracking Analysis (NTA) was performed at 20°C using a Nanosight NS300 (Malvern Instruments, Malvern, United Kingdom) equipped with a Nanosight syringe pump. The principle of NTA is based on the tracking of individual particles in suspension. A large dilution (40000 times) was necessary to meet the optimal settings of the apparatus, *i.e.* 20 – 100 particles per frame during the measurement combined to a dark background image. A syringe was loaded with the diluted suspension, the focus was adjusted manually, the infusion rate was set to 20, the camera level to 12 and 5 video images of 60 s recorded. The video images of the movement of particles under Brownian motion were analyzed by the NTA image analysis software (V 3.0 0064., Malvern Instruments). The minimum screen gain, and detection threshold of 3 were selected to maximize the detection of small particles (< 50 nm diameter). The particle size distributions obtained (data not shown) were fitted with a log-normal population of particles using Schulz equation (Schulz, 1935):

$$W(R, r_{NTA}, \sigma) = \frac{R^Z}{\Gamma(Z+1)}\left(\frac{Z+1}{r_{NTA}}\right)^{Z+1} \times exp\left[-\frac{R}{r_{NTA}}(Z+1)\right]$$

Where r_{NTA} is the average radius of the particles and Z relates to the polydispersity (σ) of the particle radii (R) given by the expression:

$$\sigma = \left(\frac{\overline{R^2}}{r_{NTA}} - 1\right) = \frac{1}{Z+1}$$

The value of σ varied from 0.23 to 0.47 within the set of suspensions and r_{NTA} was further used in the statistical analyses.

2.5.5 Cryogenic Transmission Electron microscopy

A thin vitrified film of casein micelle suspension was prepared as described in the method of (Chen et al., 2011). A Formvar lacey carbon film mounted on a 300 mesh copper grids (ProSciTech, Queensland, Australia) were glow discharged for 15 s and used as a hydrophilic support on which the suspensions (4 µL) were adsorbed. After 30 s, the grids were plunged in liquid ethane using a Vitrobot (FEI Company, Eindhoven, Netherlands) to freeze the sample. The grids were observed on a Technai G2 TF30 (FEI company, Eindhoven, Netherlands) operating at 200 kV and equipped with a Gatan US1000 2kX2k CCD Camera (Gatan). Between 10 and 20 micrographs per suspension were recorded under low-dose conditions with defocus values of 4 - 6 µm. Image analysis was performed using ImageJ software (National Institute of Health, USA). Due to the large numbers of samples, this process was automated through the use of macros set up within Image J. In total, between 1554 particles within suspension TEM and 29 092 particles within suspension B were measured in three steps:

i) The region of interest (ROI) was defined:

Particle detection was strictly limited to the area free from the grid structure and ice particles present as a result of sample preparation.

ii) Particle detection:

To detect particles, the background was subtracted from images using a ‘rolling ball’ algorithm and smoothed using Gaussian filtering before the threshold was applied and particles measured. Touching particles were separated using the distance transform watershed plugin (Quasi-Euclidean). Most of the very large particles (diameter > 50 nm) were often partially hidden by the grid. Therefore, the grid-obstructed particles were excluded from the detection only if more than 10% of the area defined by the best-fitted ellipse drawn around the particle was hidden under the grid. In order to prevent any misrepresentative segmentation, which can be caused from automatic detection, all segmentation results were visualized and the overlay was saved as a separate image that was manually inspected.

iii) Shape measurement of the particles:

Feret's diameter was determined for each particle detected. Particles were defined as small (< 50 nm in Feret's diameter) or large (> 50 nm in Feret's diameter). The ratio of small to large particles was then calculated for each suspension and defined as $\Gamma_{s/l}$.

2.5.6 Small angle X ray scattering measurements, data treatment and modelling

The SAXS measurements were carried out on the suspensions and their respective diffusible phases at the SAXS/WAXS beamline of the Australian Synchrotron (Clayton, Melbourne, Australia). The beamline is equipped with a Pilatus 1 M detector (170 mm x 170 mm, effective pixel size of 172 x 172 µm). Each sample was measured at sample-to-detector lengths of 7.106 m and 0.721 m with respective photon energies of 8.2 keV (1.512 Å) or 18.1 keV (0.685 Å). Merging the data from both distances provided a q range of 1.3 10^{-3} to 1.93 $Å^{-1}$. The samples were drawn into a 1.5 mm glass capillary; allowing continuous flow through the X-ray beam during measurements. The data were obtained from at least 10 exposures of 2 s intervals at 20°C. The capillary was rinsed with water, followed by 8 M guanidine and again with water before being air-dried between each sample analysis.

The SAXS intensities were normalized to an absolute scale and at least 10 measurements per sample were averaged to obtain the intensity profiles using ScatterBrain (V 2.71) (Australian Synchrotron, Clayton, Australia). Measurements of the diffusible phases for each suspension were subtracted from the corresponding scattering intensities of the suspensions to account for background. Finally, the intensities were adjusted to account for the difference in total protein content of the suspensions in Primus (V 3.2) (ATSAS, Hamburg, Germany). Igor software (V 7.0.2.2) (Wave Metrics, Lake Oswego, USA) was used to merge the data from the 7.106 and 0.721 m detector distances to obtain the final curves I = f(q).

The SAXS scattering intensity curves were fitted according to the model of Bouchoux et al., (2010) with slight modifications. This model considers three populations of particles: Population A, observed at low q (up to 6 x 10^{-3} $Å^{-1}$) where the scattering intensity corresponds to the presence of casein micelles; population B, in the intermediate q regions (6 x 10^{-3} to 2 x 10^{-2} $Å^{-1}$),

where the scattering corresponds to dense regions inside the casein micelles and population C; at high q (7-8 x 10^{-2} $Å^{-1}$) attributable to the CaP nanoclusters. The intensity depends on the form factor of each population $P_n(q)$ (approximated by the form factor of polydisperse spheres of mean radius r_a, r_b and r_c) and on prefactors a, b and c:

$$I(q) = a\,P_a(q) + b\,P_b(q) + c\,P_c(q)$$

with:

$$a = \alpha \times n_a\,(Vma\ \times\ \Delta\rho_a)^2$$

$$b = \alpha \times n_b\,(Vmb\ \times\ \Delta\rho_b)^2$$

$$c = \alpha \times n_c\,(Vmc\ \times\ \Delta\rho_c)^2$$

where n_a, n_b, n_c were the number of scatterers for each population, Vma, Vmb, Vmc their volume and $\Delta\rho_a$, $\Delta\rho_b$, $\Delta\rho_c$ their contrast, respectively.

The absolute number of casein micelles was assumed to be the same in all the suspensions. This hypothesis is based on the observations of Moitzi, Menzel, Schurtenberger, & Stradner, (2011) that a decrease in pH left the number of casein micelles unmodified, even if some casein micelle materials are subdivided into individual monomers or smaller casein aggregates with a resulting decrease in micelle size and mass. In the present study, it was also assumed that the modifications of the pH and the addition of NaCl and $CaCl_2$ applied in the experimental design were not sufficient to cause the complete disruption of the micellar structure. This implies that the n_a value is not affected by the physical-chemical modifications of our samples. We chose to set it to 1 so that n_b and n_c are defined relatively to one casein micelle. As a consequence, the constant α accounts for both the electron scattering length and the absolute number density of casein micelles in the samples.

This model was tested on our data according to the procedure of Bouchoux et al., (2010). First, the value of the radius of each population, r_a, r_b and r_c, and the prefactors, a, b, c, were determined by fitting the model to the experimental data with polydispersities set to σ_a = 1/3, σ_b = 1/3 and σ_c = 0.2. In a second step, the value of the constant α was calculated from the control

sample (CTRL) using the prefactor a obtained from the fit, the size (and therefore volume) of the micelle in this case, and the contrast $\Delta\rho_a$ of a native casein micelle in water, i.e. 0.018 e- $Å^{-3}$ (ρ_{water} = 0.334 e- $Å^{-3}$ and $\rho_{caseinmicelle}$ = 0.352 e- $Å^{-3}$).

In a third step, the values of $\Delta\rho_a$, n_b and n_c were calculated for the 27 suspensions using the sizes and prefactors obtained from the fits. The micelle, $\Delta\rho_a$ was simply calculated from prefactors a and sizes r_a, knowing that n_a = 1. The number of dense regions n_b was calculated from prefactors b, sizes r_b, and making the assumption that contrast $\Delta\rho_b$ is relatively insensitive to the physical-chemical modifications performed in this study. $\Delta\rho_b$ is taken as 0.035 e- $Å^{-3}$, i.e. twice the contrast of the micelle assuming that dense regions occupy 50% of the total volume of the casein micelle (Bouchoux et al. (2010)). The CaP nanoclusters / Protein inhomogeneities, n_c was calculated from prefactors c, sizes r_c, and an estimated contrast $\Delta\rho_c$ of 0.172 e- $Å^{-3}$ that was also assumed to be constant between samples. Note that in a recent work, Ingham et al., (2016) suggest a new interpretation and assign the high q features of SAXS data to the presence of inhomogeneous protein structures of 1-3 nm length scale instead of CaP nanoclusters. As our purpose is not to take a position on this question, we decided not to restrict our analysis solely to the interpretation of Bouchoux et al. (2010). A number of possible inhomogeneities n_{cPI} was therefore calculated following Ingham's postulate, this time using an estimated contrast of 0.126 e- $Å^{-3}$ (Ingham et al., 2016).

2.5.7 Rennet coagulation properties

The coagulation properties of samples were assessed using a ChymoGRAPH® (Chr Hansen, Denmark) which uses a similar physical principal to the Formagraph (McMahon & Brown, 1982). The RCT corresponded to the time elapsed from chymosin addition to the detectable onset of gelation, where gelation was defined as at the time point when the firmness of the suspensions was > 0. The maximal firmness recorded during the 60 min duration of the experiment was defined as the firmness of the gel.

2.5.8 Statistical treatments

As mentioned in section 2.3., a complete experimental design was carried out to study the combined effects of variation in pH (5.7, 6.3, 6.9), NaCl addition (0, 50, 100 mmol kg^{-1}) and $CaCl_2$ addition (0, 7.5, 15 mmol kg^{-1}) on the colloidal and renneting properties of the casein micelles (Fig. 1). The data set was subjected to statistical analysis by principal component analysis (PCA) using the Facto-MineR package and the R software (Lê, Josse, & Husson, 2008) to highlight the correlations between the different measurements. All the correlations mentioned in the results and discussion section were found to be significant ($p < 0.05$) using the paired student t-test.

In addition, multiple linear regression was also applied to the SAXS variables r_a, n_b and n_{cCaP}, using the software STATGRAPHICS Centurion XVII (V. 17.1.10, Statpoint Technologies, The Plains, USA) in order to evaluate the effect of these structural features on the firmness of the gel. A model of firmness was defined that included the quadratic effects of r_a, n_b and n_{cCaP} and the second order interactions between these factors. The full equation of the model was:

$$Firmness = constant + r_a + n_b + n_c + r_a^2 + n_b^2 + n_c^2 + (r_a \times n_b) + (r_a \times n_c) + (n_b \times n_c)$$

The LS-means were calculated and differences regarded as significant for $p < 0.05$. Non-significant effects were excluded from the model, except when first order effects were participating in interaction effects.

3 Results and discussion

The results of the biophysical analyses are presented and discussed in two main sections. In the first section, the PCA analyses are used to (i) assess the impacts of variation in pH and the addition of NaCl and $CaCl_2$ on the mineral balance of the casein micelle, (ii) establish relationships between the structure of the casein micelle and its other colloidal properties. In the second section, the relationships between rennet coagulation properties and colloidal and structural features of casein micelle are considered. Here, the PCA analyses are able to explain

317 the variation observed in RCT, while linear regression is able to explain interactions between the
318 structural properties and the firmness of the rennet gels.

319 **3.1 Colloidal and structural properties of the modified casein micelles**

320 It was found that almost 80% of the variability observed within our experimental design could be
321 evaluated by considering the first four principle components of the PCA analysis (Figs. 2 and 4).
322

323 **3.1.1 Impact of the environmental modifications on the mineral balance of the casein**
324 **micelle**

325 Analysis of the partition of minerals Ca, Pi, Na and Cl between the colloidal and diffusible
326 phases of the suspensions (Table 1) revealed that the colloidal ions consisted mainly in Ca and
327 Pi, whereas Na and Cl were mainly present in the diffusible phases of the suspensions when
328 NaCl was added. Figure 2 shows the strong, positive correlations between the pH and colloidal
329 Ca and Pi (0.85 and 0.80, respectively) and a negative correlation with the concentration of
330 diffusible Pi (- 0.86). The diffusible Ca concentration was weakly, but still significantly, impacted
331 by variation in pH, with a correlation coefficient of - 0.5 (Fig. 3).
332 The strongest variation of Ca in the diffusible phase was attributed to the addition of $CaCl_2$, with
333 a correlation coefficient of 0.84 (Fig. 4). Colloidal and diffusible concentrations of Pi were also
334 significantly impacted by the addition of $CaCl_2$ but to a much smaller extent, with correlation
335 coefficients of 0.42 and - 0.42 respectively (Fig. 3). These results confirm that modifications in
336 pH and $CaCl_2$ induced opposite effects on the mineral content of the casein micelle, with pH
337 inducing a stronger effect compared to $CaCl_2$ addition.
338 A decrease in pH led to the solubilization of the CaP nanoclusters, which has been reported in
339 the literature (Dalgleish & Law, 1989; Daviau, Famelart, Pierre, Goudrdranche, & Maubois,
340 2000; Famelart, Lepesant, Gaucheron, Le Graet, & Schuck, 1996; Le Graet & Brulé, 1993; Le
341 Graet & Gaucheron, 1999; Le Ray et al., 1998; van Hooydonk, Boerrigter, & Hagedoorn, 1986;
342 Zoon, van Vliet, & Walstra, 1989). Conversely, the addition of $CaCl_2$ limited CaP solubilization

presumably by shifting the Ca^{2+} equilibrium through the saturation of the diffusible phase (Moitzi et al., 2011). Added Ca would also directly associate with caseins and/or with the diffusible Pi and precipitate as CaP (Le Ray et al., 1998; Philippe, Le Graet, & Gaucheron, 2005; Philippe, Gaucheron, Le Graet, Michel, & Garem, 2003; Udabage, McKinnon, & Augustin, 2000).

The addition of NaCl positively correlated with the diffusible Na and Cl concentrations (0.99 and 0.95, respectively) (Fig. 2), which was consistent with the presence of NaCl in the diffusible phase. No significant correlation was found between NaCl addition and the concentrations of colloidal ions (Fig. 2) i.e. NaCl had no direct effect on the mineral content of the casein micelle within the range studied (0 to 100 mmol kg^{-1}). This result is in agreement with the finding of Karlsson, Ipsen, & Ardö (2007) who reported no change in the colloidal CaP content. However, this observation differs from the results of (Aoki, Umeda, & Nakao, 1999; Famelart et al., 1996; Grufferty & Fox, 1985; Zhao & Corredig, 2015; Zoon et al., 1989) who reported that solubilization of Ca, and occasionally Pi, occurred when NaCl was added to fresh or reconstituted skim milk or casein micelle suspensions. These discrepancies could arise from differences in pH, as in most cases, variations in pH induced by NaCl addition were not corrected, and/or the amount of added NaCl was 3 to 5 times higher than in the present study.

3.1.2 Consequences on the structural properties of the casein micelle

As mentioned in the section 2.5.6 of this paper, the SAXS data presented in Fig. 5 were treated primarily using the sponge-like model defined by Bouchoux, Gésan-Guiziou, Pérez, & Cabane, (2010) which uses three populations to interpret the SAXS pattern of casein micelles. The alternate interpretation of Ingham et al., (2016) also defines three population but attributes population C; at high q (7-8 x 10^{-2} $Å^{-1}$), to protein inhomogeneties rather than the CaP nanoclusters. Given that we have decided not to rely exclusively on the interpretation of either Ingham et al., (2016) or Bouchoux et al., (2010), the implications of the both of these studies are discussed here. The SAXS patterns (Fig. 5) show variability in the intensity of signal across these 3 different regions for the set of 9 selected samples. The structural features determined

from the SAXS data (r_a, $\Delta\rho_a$, r_b, n_b, r_c, n_c) for the 27 suspensions were compared to the other physico-chemical variables (concentrations of colloidal and diffusible minerals, τ, r_{nano}, $\Gamma_{s/l.}$...) for each population of scatterers (A, B and C) and analysed by PCA (Figs. 2, 3, 4). These correlations and the relevance of the two SAXS models applied are discussed in the following sections.

3.1.2.1 Population A: the casein micelle

The modelling of the SAXS data enabled 2 variables, r_a and $\Delta\rho_a$, describing the casein micelle radius and its contrast to be defined, respectively. The radius, r_a varied from 41.5 to 58.1 nm (Table 2), which is consistent with values determined in earlier characterizations of milk or casein micelle dispersions by SAXS (Bouchoux et al., 2010; Ingham et al., 2016; Pignon et al., 2004; Shukla et al., 2009). r_a positively and strongly correlated with the mean micellar radius measured by NTA, r_{NTA} ($53.8 < r_{NTA} < 74.8$ nm) and the turbidity, τ ($12.6 < \tau < 43.8$) of the different suspensions (Fig. 2 and Table 2), with correlation coefficients of 0.72 and 0.70, respectively. Major differences were found when comparing these radii to the values found by Tran Le, Saveyn, Hoa, & Van der Meeren (2008) for NPC dispersed in water (diameter of 212 nm). This discrepancy could arise from strong differences in the conditions of analysis (*e.g.* higher dilution of x 40 000 for our suspensions compared to x 6 000 for Tran et al. (2008), or different threshold settings).

The PCA also suggests a dependency between the micellar size and mineral balance. Indeed, r_a showed negative correlations with colloidal concentrations of Ca and Pi (- 0.71 and - 0.38, respectively) and a positive correlation with the concentration of diffusible Pi (0.38) (Fig. 2). The solubilization of the micellar CaP caused by a decrease in pH resulted in an increase in micellar size due to swelling. This size increase also affected the turbidity of the suspensions that increased (correlation coefficient of - 0.46 between pH and τ) (Fig. 2). These results were in agreement with those of Daviau et al., (2000) and van Hooydonk et al., (1986) but differed to the observations of Moitzi et al., (2011) and Ouanezar, Guyomarc'h, & Bouchoux, (2012). Indeed,

these last authors reported a decrease of micellar diameter, measured by multiple angle 3D light scattering or by AFM microscopy, respectively. In these studies, skim milk and casein micelle powders were resuspended in deionised water or synthetic milk ultrafiltrate (lactose free saline solution), respectively, providing a different ionic environment for the casein micelles than in our study. In addition, the pH ranges covered in these studies were lower than in our study and this could result in different behavior when the colloid is exposed to more severe conditions. $CaCl_2$ addition had no impact on r_a (Fig. 3), which was in agreement with results reported by Philippe et al., (2005); Philippe et al., (2003) and Udabage et al., (2000). Conversely, the concentrations of NaCl and diffusible Na significantly correlated with r_a (- 0.46, - 0.43, respectively) (Fig. 2), with NaCl addition slightly reducing the diameter of the casein micelle. This differs from the findings of Zhao & Corredig, (2015) and Karlsson, Ipsen, Schrader, & Ardö, (2005), where an increase in the size of casein micelles was observed. It is possible, however, that in these previous studies, the increase in size was due to the decrease in pH (not corrected) induced by NaCl addition rather than the direct effect of the soluble NaCl salt. Here, τ negatively correlated with NaCl (- 0.46) (Fig. 2), reflecting a decrease in scattering following NaCl addition. This result was in accordance with the two studies cited above and could be caused by a decrease in micellar size and/or internal rearrangements of the micelle structure. Diffusible Na may screen the negative charge on κ-casein CMP, causing a partial collapse of the hairy layer and a slight decrease in micellar size. The impact of NaCl on the size and turbidity of the casein micelles could also be related to the release of small casein aggregates (dense regions) from casein micelles. This argument is developed further in section 3.1.2.2 of the present paper. $\Delta\rho_a$, defined as the contrast of the casein micelle, corresponds to the electron density of the micelle (ρ_{CM}) relative to the electron density of the diffusible phase (ρ_{DF}), which consists of water containing ions (Ca, Na, Cl and Pi) from the NPC powder and/or the addition of NaCl and $CaCl_2$. The contribution of these diffusible ions to ρ_{DF} ranged from 0.02 to 0.73 %, and thus, was not taken into account here and ρ_{DF} was considered constant and equal to the electron density of

water, (0.334 e^{-} $Å^{-3}$). Therefore, in the present study, $\Delta\rho_a$ directly reflected the variation of the electron density of the casein micelle. This value depended on the volume, the casein concentration and the CaP content of the casein micelles. $\Delta\rho_a$ varied between 0.010 and 0.018 e^{-} $Å^{-3}$ (Table 2), which is of same order of magnitude as the contrast of a native casein micelle described by Bouchoux et al., (2010) and Ingham et al., (2016). $\Delta\rho_a$ presented a negative correlation (-0.86) with r_a (Fig. 2). It also positively and strongly correlated with concentrations of colloidal Ca and Pi (0.90 and 0.67, respectively) (Fig. 2). These results were consistent with an increase in the volume of the casein micelle due to a depletion in CaP, leading to a decrease in the electron density of the micelle.

3.1.2.2 Population B: the dense regions

The scattering caused by population B is characterized by r_b, the radius, and n_b, the number of dense regions per casein micelle. Both features showed variability within the full sample set, with RSD's of 38.9 and 84.1 %, respectively (Table 2). PCA analysis (Fig 2.) indicates a strong and positive correlation (0.73) between n_b and Γs/l, the ratio of small (< 50 nm in Feret's diameter) to large (> 50 nm in Feret's diameter) particles detected on cryo-TEM micrographs (section 2.5.5) (Fig. 6).

Large black and homogeneous strands crossing the cryo-TEM micrographs (Fig. 6) correspond to the grids that support the suspensions and large circular spots (*e.g.* suspension E) or merged spots (*e.g*. suspension D) were individual casein micelles and aggregates of casein micelles, respectively. Differences in the granularity of the background of the images were attributed to the presence of small-dissociated parts of the casein micelle that were present in the diffusible phase. This feature was directly quantified by the ratio $\Gamma_{s/l.}$. Image analysis revealed that these small particles have diameter of around 5 nm (around the resolution limit of the TEM microscope) to 50 nm (data not shown), which was is agreement with the size range of the population B modelled by SAXS measurements (from 6.1 nm to 21.9 nm in radius – Table 2).

This observation suggests that the dense regions detected by SAXS were not only present inside the micelle but also outside the casein micelle in the diffusible phase.

A positive correlation of 0.49 was also observed between n_b and both NaCl and diffusible Na (Fig. 2), indicating that NaCl addition increased n_b. Conversely, enrichment of the suspensions with $CaCl_2$ weakly but significantly, reduced n_b (correlation coefficient of - 0.39) (Fig. 7). Small particles of around 20 nm in diameter were also observed by Müller-Buschbaum, Gebhardt, Roth, Metwalli, & Doster (2007) using atomic force microscopy under similar conditions. These authors reported a decrease of the number of small particles in the presence of increasing Ca, consistent with observations here. To date, only the present study and that of Müller-Buschbaum et al., (2007) report the presence of dissociated aggregates outside of the casein micelle based on observations by microscopy and SAXS. It is reasonable to assume, however, that such small particles would not sediment by ultracentrifugation and a parallel can be established between our observations and the increasing presence of caseins in the supernatant obtained by ultracentrifugation, defined as soluble caseins. Our observations are also consistent with (Famelart et al., 1999; Zhao & Corredig, 2015), who reported an increase in the concentration of soluble casein after NaCl addition. Conversely, (Famelart et al., 1999; Philippe et al., 2005; Udabage et al., 2000) observed a decrease in soluble caseins when $CaCl_2$ was added. This may be explained by considering the actions of these two ions. NaCl would be responsible for the disruption and loosening of the internal structure of the casein micelle by neutralizing negative charges on the casein chains, whereas $CaCl_2$ would either favor the creation of new bonds between the phosphorylated caseins and/or prevent the dissociation of casein materials by limiting the solubilization of CaP nanoclusters. Our finding of an increase in soluble casein due to pH-induced dissociation of CaP nanoclusters is also consistent with reports by Dalgleish & Law, (1989); Le Graet & Gaucheron, (1999);and van Hooydonk et al., (1986).

In the present study, there was no significant correlation between pH and n_b (Fig. 2). pH, There was however, a direct and strong effect of pH on n_{cCaP} (the number of population C scatterers per micelle, correlation of 0.81), which correlates negatively with n_b (- 0.45) (Fig. 2). $CaCl_2$ addition had no significant impact on the size of the dense regions (Fig. 7), while NaCl caused their decrease, as shown by the correlation between $r_{b,}$ and the concentration of NaCl and therefore diffusible Na and Cl (- 0.50, - 0.53 and - 0.45, respectively) (Fig. 2). The decrease of population C also led to a decrease in size of the dense regions (correlation coefficient of 0.47 between n_{cCaP} and r_b) (Fig. 2). Finally, it is interesting to note that n_b and r_b were inversely correlated (- 0.59) (Fig. 2), meaning that the more dense the regions within the micelle, the smaller the size of these regions.

3.1.2.3 Population C: CaP nanoclusters or protein inhomogeneities

The mean radius of population C (r_c) ranged from 1.5 to 1.7 nm, for the set of suspensions studied with a RSD of 3.1 % (Table 2). This indicates that this population is of similar size in each suspension, regardless of the physico-chemical modifications applied. However, the number per casein micelle, n_{cCaP}, varied from 75 to 244. Considering this population as CaP, the number is lower than the values of CaP nanoclusters in a native casein micelle of 355 ± 20 $CaHPO_4.2H_2O$ unit reported by Holt, Timmins, Errington, & Leaver, (1998). In our experiments, the suspension of NPC powder in water caused ~20 % of the colloidal CaP to dissolve (calculated based on the colloidal and diffusible contents of the CTRL sample (Table 1) and this reduction in CaP could explain the discrepancy with the data of Holt and colleagues. The number observed, however, is consistent with the findings of Bouchoux et al., (2010), who reported ~210 CaP nanoclusters per casein micelle.

If the population C scatterers were considered as protein inhomogeneities, their number per casein micelle varied from 140 to 453, which is about 17 times lower than the value found by Ingham et al., (2016) (Table 2). This difference may be due to the application of a simple sphere form factor in this study compared to the combination of a Sorensen form factor and hard sphere

structure factor used by Ingham et al., (2016). Our approach was nevertheless sufficient to fit the SAXS pattern in the high q-region (Fig. 5). The properties of the C-scatterers *i.e*. constant size and varying number of C-scatterers per casein micelle indicated the disappearance of this population adhered to an "all-or-nothing" rule, where population C either "dissolved" completely upon modification of the environment or remained intact within the casein micelle.

According to the PCA analysis, n_{cCaP} correlated highly with: pH (0.80), concentrations of colloidal Ca and Pi (0.86 and 0.80, respectively) and with concentration of diffusible Pi (- 0.84) (Fig. 2), indicating that the high q feature disappeared with the pH-induced dissolution of colloidal CaP. Similar pH induced changes in SAXS patterns of casein micelles were reported by Ingham et al., (2016) and Marchin et al., (2007). The disappearance of the high q feature was also observed when colloidal CaP was removed from the casein micelle by the use of chelating agents (EDTA or Na_3Cit) (Day et al., 2017; Ingham et al., 2016; Marchin et al., 2007; Pitkowski, Nicolai, & Durand, 2007). These correlations are therefore consistent with the assignment of this population as CaP nanoclusters, as suggested by (Holt, de Kruif, Tuinier, & Timmins, 2003).

The correlations between n_{cCaP} noted above are not inconsistent, however, with the hypothesis of Ingham et al. (2016) *i.e.* that this population of particles corresponds to protein inhomogeneities. In this case, protein inhomogeneities would be closely linked to micellar CaP. Dissolution of the CaP from the casein micelle would also induce the disruption of the protein inhomogeneities. Such an arrangement would be in agreement with the dual binding model of (Horne, 1998), that considers CaP nanoclusters not only as crosslinking agents but also as charge neutralizers between casein chains that allow proteins to form more hydrophobic interactions. Further analysis in the form of cross comparisons between the evolution of the high q SAXS shoulder and the specific intensity variation at q = 0.035 $Å^{-1}$ observed either in SANS or resonant X-ray scattering would bring interesting information about this CaP nanocluster / protein inhomogeneity dependency. Finally, n_{cCaP} correlated negatively with n_b (- 0.45) and with $\Gamma_{s/l}$ (-0.43), and correlated positively with r_b (0.47) (Fig. 2). These weak but significant

correlations suggest that casein micelles depleted in population C released more dense regions into the diffusible phase.

3.2 Coagulation properties of the modified casein micelles

The RCT and the maximum firmness of the gel, defined here as firmness, were determined for the 27 suspensions using data obtained from the firmness curves (Fig. 8). These two parameters were linked to the other colloidal and structural variables through PCA and multiple linear regression analyses.

3.2.1 Rennet clotting time

The use of rennet made the 27 suspensions clot between 1.1 to 42.4 min (RSD of 113.5%) (Table 3). This large variability was first ascribed to the variation in pH, as there was a significant correlation between RCT and pH with a coefficient of 0.69 (Fig. 2). A consequence of the pH decrease was the solubilization of the micellar Ca and Pi (section 3.1.1). Therefore RCT also positively correlated with the concentration of colloidal Ca and Pi, and with diffusible Pi with coefficients of 0.49, 0.61 and - 0.61, respectively (Fig. 2). A reduction in RCT as a result of a decrease in pH has been well described in the literature (Choi et al., 2007; Daviau et al., 2000; Karlsson et al., 2007; Zoon et al., 1989). This has been ascribed to the enhancement of enzyme activity and a decrease in the electrostatic repulsion between paracaseinates at low pH that favored aggregation.

A weaker but significant and positive correlation was also observed between diffusible Na and RCT (0.39) (Fig. 2), meaning that an increased concentration of this ion in the diffusible phase led to an increase in the RCT. Similar effects of added NaCl have been also reported by (Bulca et al., 2016; Famelart et al., 1999; Grufferty & Fox, 1985; Karlsson et al., 2007; Sbodio et al., 2006; Zhao & Corredig, 2015; Zoon et al., 1989) and were attributed to a decrease in the rate of the rennet enzyme due to the screening of charges on κ-casein and the enzyme.

548 The negative correlations of RCT with τ and r_a (- 0.47 and – 0.53, respectively) (Fig. 2) indicated
549 that large micelles clotted more quickly than small ones, a finding that was opposite to those
550 made in the studies of Ekstrand, (1980) and Ford & Grandison, (1986). The increase of the
551 micellar size in the present study was a consequence of the pH decrease that caused the
552 micelles to swell. The correlation between these two factors is probably a disguised effect of the
553 pH. In the two studies with opposing findings, the micelles were fractionated according to their
554 size by ultracentrifugation and did not undergo any physico-chemical treatment, potentially
555 explaining these differences.

556 **3.2.2 Maximum firmness of the rennet gel**

557 Although the firmness was highly variable, with an RSD of 34 % (Table 3) within the set of
558 suspensions, this variable did not correlate directly with the other colloidal and structural
559 characteristics of the casein micelle suspensions. Indeed, the firmness, concentrations of $CaCl_2$
560 and concentrations of diffusible Ca were the only well-projected variables as defined by the 3rd
561 and 4th dimensions of the PCA analysis (Fig. 4). Vectors representing concentrations of $CaCl_2$
562 and diffusible Ca were orthogonal to the vector for firmness, reflecting no correlations between
563 these variables. However, PCA estimates the first order correlations between variables, and
564 does not take into account the interactions that might exist between the different features.
565 A second statistical approach, multiple linear regression, was therefore used to assess the effect
566 of possible interactions between variables on the firmness of the rennet gels. Structural SAXS
567 features revealed to be excellent candidates for this complementary analysis for two reasons.
568 Firstly, these variables were unique and interesting descriptors reporting information at three
569 different structural levels: 1) the casein micelle, 40 to 60 nm in radius and previously described
570 as population A; 2) the dense regions, 6 to 22 nm in radius and previously described as
571 population B; 3) the CaP nanoclusters (or protein inhomogeneities), 1.5 to 1.7 nm in radius and
572 previously described as population C. Secondly, these variables correlated significantly with the
573 whole set of colloidal and mineral features determined by other techniques and constituted a

574 way to summarize the whole set of data. Therefore, r_a, n_b and n_{cCaP} were subject to linear
575 regression in order to define a predictive model of the firmness that considered the quadratic
576 effects and the second order interactions between these variables. For consistency, the values
577 of n_{cCaP} used in this statistical analysis were determined considering population C as CaP
578 nanoclusters. This would make no difference in the properties of the model, as there was a
579 proportional relationship linking n_{cCaP} for CaP nanoclusters and n_{cPI} for protein inhomogeneities.
580 Based on the experimental design, the following model equation was established to predict the
581 maximum firmness of the rennet gels made from the suspensions:

$$Firmness = 187.3 - 3.5 \times ra - 1.2 \times n_b - 0.9 \times n_{cCaP} + 0.02 \times (r_a \times n_c)$$

582 where r_a was the radius of the casein micelle, n_b and n_{cCaP} were the number of dense regions
583 and CaP nanoclusters per casein micelle, respectively. This model explained 68.5% of the
584 variability of the firmness. Statistical analysis also revealed that the interaction between r_a and n_c
585 (r_a x n_c) and the first order effect of n_b in this model were significant. These two contributions
586 had a statistical weight of 35.3% and 27 % in the model, respectively.
587 Figure 9.A and B. displays each suspension in the first four dimensions of the PCA. The
588 suspensions are colored according to their firmness (orange for weak, red for medium, black for
589 strong). Figure 9.A represents the evolution of firmness within the set of samples, defined by
590 PCs 3 and 4 with the arrow pointing in the direction of increasing firmness (the same direction as
591 seen in Figure 4). The negative coefficient assigned to n_b in the firmness equation model
592 indicates that the release of dense regions from the casein micelles led to the formation of
593 weaker gels. This direct effect is well illustrated when reading Figure 9.A from the bottom right
594 corner (suspension G, U - poor in dense regions and stronger gels) to the upper left corner
595 (suspension B - rich in dense regions and a weaker gel).
596 As mentioned in section 3.1.2.2, the release of dense regions was favored by the addition of
597 NaCl and limited by the addition of $CaCl_2$. The influence of NaCl on the firmness has been
598 examined by several groups but conflicting results have been reported. Consistent with the

599 results reported here, Famelart et al., (1999) and Grufferty & Fox (1985) did not observe any
600 modification of the moduli or the curd tension of the rennet gels upon addition of NaCl. However,
601 Bulca et al., (2016) and Zhao & Corredig, (2015) reported a decrease in the firmness or stiffness
602 of the rennet gels. While Zoon et al., (1989) observed higher moduli for 8h aged gels
603 supplemented in NaCl but lower moduli only 1h after the addition of rennet to the milk, which
604 corresponded to the experimental conditions of the present study. The negative effect of NaCl
605 on the firmness of rennet gels is poorly explained in the literature. A competition between Na^+
606 and Ca^{2+} has been proposed, as well as the screening of casein charges and in some cases, the
607 solubilization of the micellar CaP (Grufferty & Fox, 1985; Zhao & Corredig, 2015). Based on the
608 significant correlations that link n_b and NaCl and the significant negative effect of n_b on the
609 firmness of the rennet gel, we would argue that the decrease in firmness observed with the
610 addition of NaCl is due to the release of dense regions from the casein micelles. This
611 explanation is similar to that of Gaygadzhiev, Massel, Alexander, & Corredig, (2012), who found
612 that the addition of sodium caseinate to milk inhibited the aggregation of casein micelles. In this
613 case the soluble dense regions may adsorb on the surface of the paracaseinate formed after
614 rennet addition, causing an increase in the steric repulsion between the rennet-altered particles
615 which would limit the aggregation phenomenon and the formation of a firm network.
616 In contrast, there is a general consensus that $CaCl_2$ addition increases gel firmness (Deeth &
617 Lewis, 2015; Sandra et al., 2012; Zoon et al., 1988). In this case, this improvement was
618 attributed to the ability of Ca to preserve the number of CaP bonds between the caseins within
619 the micelle but also within the casein gel network. It was demonstrated in section 3.1.2.2, that
620 $CaCl_2$ addition limited the release of dense regions, which consequently had a positive impact
621 on the firmness of the gels through the decrease of n_b.
622
623 The effect of the interaction between r_a and n_{cCaP} appears to be more subtle. The direct effect of
624 r_a could be seen in figure 9.B from the upper right corner (suspension M - small casein micelle)

to the bottom left corner (suspension A, D, O - large and swollen casein micelle). There were no direct and simple consequences of r_a on the gel firmness. This can be illustrated by the medium size micelles (center of the graph, suspensions B, S, V, L for instance) that can either form weak, medium or strong gels. This result was quite consistent with the observation of Dalgleish, Brinkhuis, & Payens, (1981) who found no dependence between the size of micelles and their coagulation. Yet, several authors have reported that small casein micelles form stronger gels (Ford & Grandison, 1986; Logan et al., 2015; Niki, Kohyama, Sano, & Nishinari, 1994). However, in these studies, the micelles were in their native state because they were either isolated from milk by ultracentrifugation or were in milk samples that were selected from cows who produced small casein micelles. In contrast, the present study involved modifications to the environment that affected the size of the casein micelles.

The direct effect of n_{cCaP} can be observed in figure 9.B from the upper left corner (suspension B – poor in population C) to the bottom right corner (suspensions L, Y – rich in population C) but no direct dependency of gel firmness on n_{cCaP} was observed. As mentioned in section 3.1.2.3, this population may be either CaP nanoclusters or protein inhomogeneities. In both cases, the presence of such interactions, whether they are mineral-protein or protein-protein interactions, would create more crosslinking points resulting in a stronger gel network.

The literature reports a quadratic relationships between pH and rennet gel firmness, *i.e.* there is a parabolic increase in the gel firmness with pH up to a maximum value, followed by a parabolic decrease in firmness (Choi et al., 2007; Karlsson et al., 2007; Lucey, Johnson, & Horne, 2003; Zoon et al., 1989). A change in pH modifies the ionization of individual amino acids, either increasing or decreasing the electrostatic interactions between casein chains. A simultaneous consequence is the solubilization of the micellar CaP at lower pH, which decreases the attractive interactions between casein molecules. The addition of a chelating agent to milk or casein suspension similarly leads to the solubilization of micellar CaP (de Kort et al., 2011; McCarthy et

al., 2017; Mizuno & Lucey, 2005; Pitkowski et al., 2007) and causes a decrease in the firmness of the rennet gels (Choi et al., 2007).

At this point, it is important to remember that the variations of r_a and n_{cCaP} were not impacted by only one factor (size fractionation, or pH, or chelating agent addition) but by the simultaneous effect of three factors (pH, NaCl and $CaCl_2$). Therefore, the firmness modeling reveals that the interaction between those variables should be considered. The interaction between r_a and n_{cCaP} on the rennet gel firmness means that the firmness at a given r_a depended on n_{cCaP} and vice versa. As an example to illustrate this interaction, suspensions containing medium sized casein micelles (from 45 to 47 nm in radius) can lead to the formation of weaker gels if the amount of C-particles is too low (suspension B). Yet these micelles formed medium strength gels (suspensions P, E, C) if their C-particle content increased, or even stronger gels when those casein micelles are rich in C-particles (suspensions X, I, T). Similarly, small casein micelles that were rich in C-particles formed weaker gels (suspension W, K, M) but an increase in micelle size led to an increase in gel firmness (suspension H, V, T). Large casein micelles, depleted in C particles (suspension A, O, D) also formed weaker gels.

4 Conclusion

The multifactorial experimental design applied here allowed the effect of three variables: pH, NaCl and $CaCl_2$ on the colloidal and rennet coagulation properties of casein micelles to be assessed and ranked. Variations in pH had the strongest influence on the mineral balance of the casein micelles. A decrease in pH caused the colloidal CaP to solubilize. In contrast, NaCl addition had no impact on the mineral content of the casein micelle. The solubilization of colloidal CaP caused the micelle to shrink while the addition of NaCl reduced the size of the casein micelle due to the release of small particles into the diffusible phase. The presence of such particles, around 25 nm in diameter, was strongly supported by experimental SAXS data combined with observations by cryo-TEM. These particles are believed to be part of the dense

676 regions described by Bouchoux et al. (2010); here they were observed both inside and outside
677 of the casein micelle. $CaCl_2$ had no effect on the casein micelle size but prevented disruption of
678 the dense regions within the micelle. The SAXS data also revealed the presence of a high-q
679 structural feature (the C-population), that were of a constant size (~1.6 nm in radius) but varied
680 in number with different environmental conditions. Their presence was strongly dependent to the
681 CaP content of the casein micelle. This feature could be assigned to the presence of either CaP
682 nanoclusters or protein inhomogeneities.
683 The renneting properties were most impacted by a decrease in pH, causing a reduction in RCT,
684 while NaCl supplementation led to longer RCT. Variations in gel firmness were more complex
685 but could be explained by considering the interactions between the size of the casein micelle,
686 the C-population and the dissociation of dense regions within the casein micelle.
687 Together the data presented here illustrate the complex interactions of three variables on the
688 properties of casein micelles, this study provides a framework that links existing literature on the
689 effect of single variables and improves our understanding of how the properties of casein
690 micelles can be manipulated to control micelle size, structure and functional properties.
691

692 **5 Acknowledgment**

693 Acknowledgements are given to François Boué for the interesting discussions regarding the
694 modeling of the SAXS data, to Arlette Leduc for assistance in the analysis of the minerals, to Mi
695 Xu for assistance with data collection at the Australian Synchrotron and the Biological Optical
696 Microscopy Platform (BOMP) at the Bio21 Molecular Science and Biotechnology Institute for
697 access to equipment.
698 Fundings: This work was supported by the French Dairy Interbranch Organization (CNIEL) for
699 their financial support and by Chr Hansen through the loan of a Chymograph®. Sally Gras and
700 Lydia Ong are supported by the Australian Research Council's Industrial Transformation
701 Research Program (ITRP) funding scheme (project number IH120100005). The ARC Dairy

Innovation Hub is a collaboration between the University of Melbourne, The University of Queensland and Dairy Innovation Australia Ltd. The SAXS experiments were undertaken on the SAXS/WAXS beamline at the Australian Synchrotron, Victoria, Australia (Proposal No. AS163/SAXS/11019).

6 References

Abdi, H., & Williams, L. J. (2010). Principal component analysis. *Wiley Interdisciplinary Reviews: Computational Statistics*, *2*(4), 433–459. https://doi.org/10.1002/wics.101

Aoki, T., Umeda, T., & Nakao, T. (1999). Effect of sodium chloride on the properties of casein micelles, *2*, 91–93.

Bouchoux, A., Gésan-Guiziou, G., Pérez, J., & Cabane, B. (2010). How to squeeze a sponge: casein micelles under osmotic stress, a SAXS study. *Biophysical Journal*, *99*(11), 3754–3762. https://doi.org/10.1016/j.bpj.2010.10.019

Bouchoux, A., Ventureira, J., Gésan-Guiziou, G., Garnier-Lambrouin, F., Qu, P., Pasquier, C., … Cabane, B. (2015). Structural heterogeneity of milk casein micelles: a SANS contrast variation study. *Soft Matter*, *11*(2), 389–399. https://doi.org/10.1039/C4SM01705F

Broyard, C., & Gaucheron, F. (2015). Modifications of structures and functions of caseins: a scientific and technological challenge. *Dairy Science & Technology*. https://doi.org/10.1007/s13594-015-0220-y

Bulca, S., Wolfschoon-Pombo, A., & Kulozik, U. (2016). Rennet coagulation properties of UHT-treated phosphocasein dispersions as a function of casein and NaCl concentrations. *International Journal of Dairy Technology*, *69*(3), 328–336. https://doi.org/10.1111/1471-0307.12308

Chen, Y.-Y., Peng, B., Yang, Q., Glew, M. D., Veith, P. D., Cross, K. J., … Reynolds, E. C. (2011). The outer membrane protein LptO is essential for the O-deacylation of LPS and the co-ordinated secretion and attachment of A-LPS and CTD proteins in Porphyromonas gingivalis:

LptO-dependent maturation of A-LPS and CTD proteins. *Molecular Microbiology*, *79*(5), 1380–1401. https://doi.org/10.1111/j.1365-2958.2010.07530.x

Choi, J., Horne, D. S., & Lucey, J. A. (2007). Effect of insoluble calcium concentration on rennet coagulation properties of milk. *Journal of Dairy Science*, *90*(6), 2612–2623. https://doi.org/10.3168/jds.2006-814

Dalgleish, D. G., Brinkhuis, J., & Payens, T. A. J. (1981). The coagulation of differently sized casein micelles by rennet. *European Journal of Biochemistry*, *119*(2), 257–261. https://doi.org/10.1111/j.1432-1033.1981.tb05602.x

Dalgleish, D. G., & Corredig, M. (2012). The Structure of the Casein Micelle of Milk and Its Changes During Processing. *Annual Review of Food Science and Technology*, *3*(1), 449–467. https://doi.org/10.1146/annurev-food-022811-101214

Dalgleish, D. G., & Law, A. J. R. (1989). pH-Induced dissociation of bovine casein micelles. II. Mineral solubilization and its relation to casein release. *Journal of Dairy Research*, *56*(05), 727. https://doi.org/10.1017/S0022029900029290

Daviau, C., Famelart, M.-H., Pierre, A., Goudedranche, H., & Maubois, J.-L. (2000). Rennet coagulation of skim milk and curd drainage: effect of pH, casein concentration, ionic strength and heat treatment. *Le Lait*, *80*(4), 397–415. https://doi.org/10.1051/lait:2000134

Day, L., Raynes, J. K., Leis, A., Liu, L. H., & Williams, R. P. W. (2017). Probing the internal and external micelle structures of differently sized casein micelles from individual cows milk by dynamic light and small-angle X-ray scattering. *Food Hydrocolloids*, *69*, 150–163. https://doi.org/10.1016/j.foodhyd.2017.01.007

de Kort, E., Minor, M., Snoeren, T., van Hooijdonk, T., & van der Linden, E. (2011). Effect of calcium chelators on physical changes in casein micelles in concentrated micellar casein solutions. *International Dairy Journal*, *21*(12), 907–913. https://doi.org/10.1016/j.idairyj.2011.06.007

753 de Kruif, C. G. (1999). Casein micelle interactions. *International Dairy Journal*, *9*(3–6), 183–188.
754 https://doi.org/10.1016/S0958-6946(99)00058-8
755 de Kruif, C. G. (2014). The structure of casein micelles: a review of small-angle scattering data.
756 *Journal of Applied Crystallography*, *47*(5), 1479–1489.
757 https://doi.org/10.1107/S1600576714014563
758 de Kruif, C. G., & Zhulina, E. B. (1996). k-casein as a polyelectrolyte brush on the surface of
759 casein micelles. *Colloids and Surfaces A: Physicochemical and Engineering Aspects*, *117*(1–2),
760 151–159. https://doi.org/10.1016/0927-7757(96)03696-5
761 Deeth, H. C., & Lewis, M. J. (2015). Practical consequences of calcium addition to and removal
762 from milk and milk products. *International Journal of Dairy Technology*, *68*(1), 1–10.
763 https://doi.org/10.1111/1471-0307.12188
764 Ekstrand, B. (1980). Casein micelle size and composition related to the enzymatic coagulation
765 process. *Biochimica et Biophysica Acta (BBA) - General Subjects*, *630*(3), 361–366.
766 https://doi.org/10.1016/0304-4165(80)90284-6
767 Famelart, M.-H., Le Graet, Y., & Raulot, K. (1999). Casein micelle dispersions into water, NaCl
768 and CaCl2: physicochemical characteristics of micelles and rennet coagulation. *International*
769 *Dairy Journal*, *9*, 293–297.
770 Famelart, M.-H., Lepesant, F., Gaucheron, F., Le Graet, Y., & Schuck, P. (1996). pH-Induced
771 physicochemical modifications of native phosphocaseinate suspensions: Influence of aqueous
772 phase. *Le Lait*, *76*(5), 445–460. https://doi.org/10.1051/lait:1996534
773 Ford, G. D., & Grandison, A. S. (1986). Effect of size of casein micelles on coagulation
774 properties of skim milk. *Journal of Dairy Research*, *53*(01), 129.
775 https://doi.org/10.1017/S0022029900024729
776 Gaucheron, F. (2004). *Minéraux et produits laitiers*. Paris: Technique & Documentation.

777 Gaygadzhiev, Z., Massel, V., Alexander, M., & Corredig, M. (2012). Addition of sodium caseinate
778 to skim milk inhibits rennet-induced aggregation of casein micelles. *Food Hydrocolloids*, *26*(2),
779 405–411. https://doi.org/10.1016/j.foodhyd.2011.02.015
780 Grufferty, M. B., & Fox, P. F. (1985). Effect of added NaCl on some physicochemical properties
781 of milk, *9*, 1–9.
782 Holt, C., Carver, J. A., Ecroyd, H., & Thorn, D. C. (2013). Invited review: Caseins and the casein
783 micelle: Their biological functions, structures, and behavior in foods. *Journal of Dairy Science*,
784 *96*(10), 6127–6146. https://doi.org/10.3168/jds.2013-6831
785 Holt, C, de Kruif, C. G., Tuinier, R., & Timmins, P. A. (2003). Substructure of bovine casein
786 micelles by small-angle X-ray and neutron scattering. *Colloids and Surfaces A: Physicochemical*
787 *and Engineering Aspects*, *213*(2–3), 275–284. https://doi.org/10.1016/S0927-7757(02)00520-4
788 Holt, C., Timmins, P. A., Errington, N., & Leaver, J. (1998). A core-shell model of calcium
789 phosphate nanoclusters stabilized by beta-casein phosphopeptides, derived from sedimentation
790 equilibrium and small-angle X-ray and neutron-scattering measurements. *European Journal of*
791 *Biochemistry*, *252*(1), 73–78. https://doi.org/10.1046/j.1432-1327.1998.2520073.x
792 Holt, C. (2016). Casein and casein micelle structures, functions and diversity in 20 species.
793 *International Dairy Journal*, *60*, 2–13. https://doi.org/10.1016/j.idairyj.2016.01.004
794 Holt, C., & Horne, D. S. (1996). The hairy casein micelle : Evolution of the concept and its
795 implications for dairy technology. *Nederlands Melk En Zuiveltijdschrift*, *50*(2), 85–111.
796 Horne, D. S. (1998). Casein interactions: casting light on the black boxes, the structure in dairy
797 products. *International Dairy Journal*, *8*(3), 171–177. https://doi.org/10.1016/S0958-
798 6946(98)00040-5
799 Horne, D. S. (2017). A balanced view of casein interactions. *Current Opinion in Colloid &*
800 *Interface Science*, *28*, 74–86. https://doi.org/10.1016/j.cocis.2017.03.009

Ingham, B., Erlangga, G. D., Smialowska, A., Kirby, N. M., Wang, C., Matia-Merino, L., … Carr, A. J. (2015). Solving the mystery of the internal structure of casein micelles. *Soft Matter*, *11*(14), 2723–2725. https://doi.org/10.1039/C5SM00153F

International Dairy Federation. (2014). Milk and milk products - Determination of nitrogen content - Part 1: Kjeldahl principle and crude protein calculation.

Ingham, B., Smialowska, A., Erlangga, G. D., Matia-Merino, L., Kirby, N. M., Wang, C., … Carr, A. J. (2016). Revisiting the interpretation of casein micelle SAXS data. *Soft Matter*, *12*(33), 6937–6953. https://doi.org/10.1039/C6SM01091A

Jolliffe, I. (2014). Principal component analysis. In N. Balakrishnan, T. Colton, B. Everitt, W. Piegorsch, F. Ruggeri, & J. L. Teugels (Eds.), *Wiley StatsRef: Statistics Reference Online*. Chichester, UK: John Wiley & Sons, Ltd. https://doi.org/10.1002/9781118445112.stat06472

Karlsson, A. O., Ipsen, R., & Ardö, Y. (2007). Influence of pH and NaCl on rheological properties of rennet-induced casein gels made from UF concentrated skim milk. *International Dairy Journal*, *17*(9), 1053–1062. https://doi.org/10.1016/j.idairyj.2007.01.006

Karlsson, A. O., Ipsen, R., Schrader, K., & Ardö, Y. (2005). Relationship between physical properties of casein micelles and rRheology of skim milk concentrate. *Journal of Dairy Science*, *88*(11), 3784–3797. https://doi.org/10.3168/jds.S0022-0302(05)73064-2

Lazzaro, F., Saint-Jalmes, A., Violleau, F., Lopez, C., Gaucher-Delmas, M., Madec, M.-N., … Gaucheron, F. (2017). Gradual disaggregation of the casein micelle improves its emulsifying capacity and decreases the stability of dairy emulsions. *Food Hydrocolloids*, *63*, 189–200. https://doi.org/10.1016/j.foodhyd.2016.08.037

Le Graet, Y., & Brule, G. (1993). Les équilibres minéraux du lait : influence du pH et de la force ionique, *73*, 51–60.

Le Graet, Y., & Gaucheron, F. (1999). pH-induced solubilization of minerals from casein micelles: influence of casein concentration and ionic strength, *66*, 215–224.

826 Le Ray, C., Maubois, J.-L., Gaucheron, F., Brule, G., Pronnier, P., & Garnier, F. (1998). Heat
827 stability of reconstituted casein micelle dispersions: changes induced by salt addition. *Le Lait*,
828 *78*(4), 375–390. https://doi.org/10.1051/lait:1998437
829 Lê, S., Josse, J., & Husson, F. (2008). FactoMineR: An R package for multivariate analysis.
830 *Journal of Statistical Software*, *25*(1). https://doi.org/10.18637/jss.v025.i01
831 Logan, A., Leis, A., Day, L., Øiseth, S. K., Puvanenthiran, A., & Augustin, M. A. (2015). Rennet
832 gelation properties of milk: Influence of natural variation in milk fat globule size and casein
833 micelle size. *International Dairy Journal*, *46*, 71–77. https://doi.org/10.1016/j.idairyj.2014.08.005
834 Lucey, J. A. (2002). Formation and physical properties of milk protein gels. *Journal of Dairy*
835 *Science*, *85*(2), 281–294. https://doi.org/10.3168/jds.S0022-0302(02)74078-2
836 Lucey, J. A., Johnson, M. E., & Horne, D. S. (2003). Invited review: Perspectives on the basis of
837 the rheology and texture properties of cheese. *Journal of Dairy Science*, *86*(9), 2725–2743.
838 https://doi.org/10.3168/jds.S0022-0302(03)73869-7
839 Marchin, S., Putaux, J.-L., Pignon, F., & Léonil, J. (2007). Effects of the environmental factors on
840 the casein micelle structure studied by cryo transmission electron microscopy and small-angle x-
841 ray scattering/ultrasmall-angle x-ray scattering. *The Journal of Chemical Physics*, *126*(4),
842 045101. https://doi.org/10.1063/1.2409933
843 McCarthy, N. A., Power, O., Wijayanti, H. B., Kelly, P. M., Mao, L., & Fenelon, M. A. (2017).
844 Effects of calcium chelating agents on the solubility of milk protein concentrate. *International*
845 *Journal of Dairy Technology*, *70*(3), 415–423. https://doi.org/10.1111/1471-0307.12408
846 Mizuno, R., & Lucey, J. A. (2005). Effects of emulsifying salts on the turbidity and calcium-
847 phosphate–protein interactions in casein micelles. *Journal of Dairy Science*, *88*(9), 3070–3078.
848 https://doi.org/10.3168/jds.S0022-0302(05)72988-X
849 Moitzi, C., Menzel, A., Schurtenberger, P., & Stradner, A. (2011). The pH induced Sol−Gel
850 transition in skim milk revisited. A detailed study using time-resolved light and X-ray scattering
851 experiments. *Langmuir*, *27*(6), 2195–2203. https://doi.org/10.1021/la102488g

852 Müller-Buschbaum, P., Gebhardt, R., Roth, S. V., Metwalli, E., & Doster, W. (2007). Effect of
853 calcium concentration on the structure of casein micelles in thin films. *Biophysical Journal*, *93*(3),
854 960–968. https://doi.org/10.1529/biophysj.107.106385
855 Niki, R., Kohyama, K., Sano, Y., & Nishinari, K. (1994). Rheological study on the rennet-induced
856 gelation of casein micelles with different sizes. *Polymer Gels and Networks*, *2*(2), 105–118.
857 https://doi.org/10.1016/0966-7822(94)90030-2
858 Ouanezar, M., Guyomarc'h, F., & Bouchoux, A. (2012). AFM imaging of milk casein micelles:
859 Evidence for structural rearrangement upon acidification. *Langmuir*, *28*(11), 4915–4919.
860 https://doi.org/10.1021/la3001448
861 Philippe, M, Le Graet, Y., & Gaucheron, F. (2005). The effects of different cations on the
862 physicochemical characteristics of casein micelles. *Food Chemistry*, *90*(4), 673–683.
863 https://doi.org/10.1016/j.foodchem.2004.06.001
864 Philippe, Marine, Gaucheron, F., Le Graet, Y., Michel, F., & Garem, A. (2003). Physicochemical
865 characterization of calcium-supplemented skim milk. *Le Lait*, *83*(1), 45–59.
866 https://doi.org/10.1051/lait:2002049
867 Pierre, A., Fauquant, J., Le Graet, Y., & Maubois, J.-L. (1992). Préparation de phosphocaséinate
868 natif par microfiltration sur membrane. *Lait*, (72), 461–474.
869 Pignon, F., Belina, G., Narayanan, T., Paubel, X., Magnin, A., & Gésan-Guiziou, G. (2004).
870 Structure and rheological behavior of casein micelle suspensions during ultrafiltration process.
871 *The Journal of Chemical Physics*, *121*(16), 8138. https://doi.org/10.1063/1.1800931
872 Pitkowski, A., Nicolai, T., & Durand, D. (2007). Scattering and turbidity study of the dissociation
873 of the casein by calcium chelation. *Biomacromolecules*, *9*, 369–375.
874 Sandra, S., Ho, M., Alexander, M., & Corredig, M. (2012). Effect of soluble calcium on the
875 renneting properties of casein micelles as measured by rheology and diffusing wave
876 spectroscopy. *Journal of Dairy Science*, *95*(1), 75–82. https://doi.org/10.3168/jds.2011-4713

877 Sbodio, O. A., Tercero, E. J., Coutaz, R., & Revelli, G. R. (2006). Effect of rennet and sodium
878 chloride concentration on milk coagulation properties. *Ciencia Y Tecnologia Alimentaria*, *5*(3),
879 182–188. https://doi.org/10.1080/11358120609487690
880 Schmidt, D. G. (1982). *Developments in Dairy Chemistry: 1. Proteins* (P. F. Fox). London:
881 Applied Science Publishers.
882 Schuck, P., Piot, M., Méjean, S., Le Graet, Y., Fauquant, J., Brule, G., & Maubois, J. L. (1994).
883 Déshydratation par atomisation de phosphocaséinate natif obtenu par microfiltration sur
884 membrane. *Le Lait*, *74*(5), 375–388. https://doi.org/10.1051/lait:1994531
885 Schulz, G. V. (1935). Highly polymerized compounds. CXXII. The relation between reaction rate
886 and composition of the reaction product in macropolymerization processes. *B30*, 379–398.
887 Shukla, A., Narayanan, T., & Zanchi, D. (2009). Structure of casein micelles and their
888 complexation with tannins. *Soft Matter*, *5*(15), 2884. https://doi.org/10.1039/b903103k
889 Silva, N. N., Piot, M., de Carvalho, A. F., Violleau, F., Fameau, A.-L., & Gaucheron, F. (2013).
890 pH-induced demineralization of casein micelles modifies their physico-chemical and foaming
891 properties. *Food Hydrocolloids*, *32*(2), 322–330. https://doi.org/10.1016/j.foodhyd.2013.01.004
892 Thorn, D. C., Meehan, S., Sunde, M., Rekas, A., Gras, S. L., MacPhee, C. E., … Carver, J. A.
893 (2005). Amyloid Fibril Formation by Bovine Milk κ-Casein and Its Inhibition by the Molecular
894 Chaperones α_S - and β-Casein. *Biochemistry*, *44*(51), 17027–17036.
895 https://doi.org/10.1021/bi051352r
896 Tran Le, T., Saveyn, P., Hoa, H. D., & Van der Meeren, P. (2008). Determination of heat-
897 induced effects on the particle size distribution of casein micelles by dynamic light scattering and
898 nanoparticle tracking analysis. *International Dairy Journal*, *18*(12), 1090–1096.
899 https://doi.org/10.1016/j.idairyj.2008.06.006
900 Tuinier, R., & de Kruif, C. G. (2002). Stability of casein micelles in milk. *The Journal of Chemical*
901 *Physics*, *117*(3), 1290–1295. https://doi.org/10.1063/1.1484379

902 Udabage, P., McKinnon, I. R., & Augustin, M. A. (2000). Mineral and casein equilibria in milk:
903 effects of added salts and calcium-chelating agents, *67*, 361–370.
904 van Hooydonk, A. C. M., Boerrigter, I. J., & Hagedoorn, H. G. (1986). pH-induced physico-
905 chemical changes of casein micelles in milk and their effect on renneting. 2. Effect of pH on
906 renneting of milk, *40*, 297–313.
907 Walstra, P. (1999). Casein sub-micelles: do they exist? *International Dairy Journal*, *9*(3–6), 189–
908 192. https://doi.org/10.1016/S0958-6946(99)00059-X
909 Wold, S., Esbensen, K., & Geladi, P. (1987). Principal component analysis. *Chemometrics and*
910 *Intelligent Laboratory Systems*, *2*(1–3), 37–52. https://doi.org/10.1016/0169-7439(87)80084-9
911 Zhao, Z., & Corredig, M. (2015). Changes in the physico-chemical properties of casein micelles
912 in the presence of sodium chloride in untreated and concentrated milk protein. *Dairy Science &*
913 *Technology*, *95*(1), 87–99. https://doi.org/10.1007/s13594-014-0200-7
914 Zoon, P., van Vliet, T., & Walstra, P. (1988). Rheological properties of rennet-induced skim milk
915 gels. 3. The effect of calcium and phosphate, *43*, 295–312.
916 Zoon, P., van Vliet, T., & Walstra, P. (1989). Rheological properties of rennet-induced skim milk
917 gels. 4. The effect of pH and NaCl, *43*, 17–34.
918

Table 1: Distribution of the mineral salts in the suspensions. Colloidal concentrations were determined by subtracting the concentration of diffusible ions from the concentration of total ions. Average, standand deviation (SD), relative standard deviation (RSD), minimum and maximum values were determined on the complete set of 27 samples.

Table 2: Size-related parameters determined by different analytical methods including Turbidimetry, NTA, SAXS and Cryo-TEM. Average, standand deviation (SD), relative standard deviation (RSD), minimum and maximum values were determined on the complete set of 27 samples. n_{cCaP} and n_{cPI} correspond to the number of C scatterers per casein micelle, in the case where these scatterers are considered as CaP nanoclusters or protein Inhomogeneities, respectively.

Table 3: Rennet coagulation properties of Firmness and Rennet Coagulation Time (RCT). Average, standand deviation (SD), relative standard deviation (RSD), minimum and maximum values were determined on the complete set of 27 samples.

Figure 1: Cubic representation of the experimental design. Each of the 27 suspension is represented by a letter or designated as CTRL (control suspension, pH 6.9, no salts added). The pH of the suspensions was set to 5.7, 6.3 or 6.9 and the suspensions contained 0, 50 or 100 mmol kg^{-1} of added NaCl and 0, 7.5 or 15 mmol kg^{-1} of added $CaCl_2$.

Figure 2: PCA showing the correlation circle of 21 variables in the plan delimited by the two first principal components (PCs). 57.8 % of the variability of the set of data is represented in this PCA plan.

Figure 3: PCA showing the correlation circle of 21 variables in the plan delimited by the first and the fourth principal components (PCs). 44.5 % of the variability of the set of data is represented in this PCA plan.

Figure 4: PCA showing the correlation circle of 21 variables in the plan delimited by the third and the fourth principal components (PCs). 21.3 % of the variability of the set of data is represented in this PCA plan.

Figure 5: Fit to the SAXS data shown in a log – log plot. The scattering curves have been translated along the y axis for clarity. The scattering profiles have been fitted using the model of Bouchoux et al. (2010) that contains 3 populations of scatterers: the casein micelle (population A - up to 6 x 10-3 $Å^{-1}$), the dense regions (population B - 6 x 10-3 to 2 x 10-2 $Å^{-1}$) and either the CaP nanocluster or the proteins inhomogeneities (population C - 7-8 x 10-2 $Å^{-1}$). Open diamonds show experimental data; the solid lines represent fits for which the parameter values are given in Table 2.

Figure 6: Cryo-TEM micrographs of the selected suspensions. Large black strands crossing the images are carbon grids, circular or merged spots are casein micelles or aggregated casein micelles. Dark round spots in suspension L are ice particles that formed during storage of the grids in liquid nitrogen. Granular backgrounds point out the presence of small casein aggregates dissociated from the casein micelles. This feature is quantified for each suspensions by a $\Gamma_{s/l}$ (ratio of small < 50 nm to large > 50 nm particles). The values of $\Gamma_{s/l}$ are reported in Table 2.

Figure 7: PCA showing the correlation circle of 21 variables in the plan delimited by the second and the fourth principal components (PCs). 33.6 % of the variability of the set of data is represented in this PCA plan.

Figure 8: Evolution of firmness as a function of time for selected samples. Arrows point to the Rennet Clotting Time (RCT) for each of the suspensions, while firmess was defined as the maximum firmness reached within 60 min of the addition of chymosin to the suspensions. Values of RCT and Firmness are reported in Table 3.

Figure 9: PCA showing the similarity of suspensions determined by A. The third and fourth Principal Components (PCs) and B. the two first PCs. Suspensions leading to weak gels are colored in orange, gels with medium firmness are red and gels with strong firmness are black. Arrows indicate the direction of correlation for firmness and SAXS variables in the same PC plans (A. see Figure 4 and B. see Figure 2).

	Diffusible Ca (mmol kg^{-1})	Colloidal Ca (mmol kg^{-1})	Diffusible Na (mmol kg^{-1})	Colloidal Na (mmol kg^{-1})	Diffusible Cl (mmol kg^{-1})	Colloidal Cl (mmol kg^{-1})	Diffusible Pi (mmol kg^{-1})	Colloidal Pi (mmol kg^{-1})
Full experimental plan - 27 suspensions								
Average	12.4	14.8	64.8	0.2	67.4	0.5	2.4	4.6
SD	6.0	4.3	45.5	0.5	45.7	1.4	1.3	1.3
RSD (%)	48.2	29.2	70.3	300.9	67.8	287.6	55.1	28.1
minimum	2.1	3.6	6.7	0.0	0.0	0.0	0.0	1.9
maximum	22.9	20.2	135.6	2.2	138.0	6.2	5.0	7.2
Selected individual suspensions								
A	9.6	8.2	8.9	0.0	2.2	1.6	3.8	3.3
B	11.0	8.8	114.4	0.0	102.7	6.2	4.8	1.9
D	20.1	12.0	24.0	0.0	26.9	3.3	2.9	3.5
E	22.8	12.3	121.7	0.0	130.7	0.0	3.4	3.5
J	3.5	15.8	120.2	0.0	94.4	0.0	1.7	4.9
L	14.7	20.2	10.5	0.0	17.9	1.8	0.8	5.4
M	16.3	18.8	135.6	0.0	129.4	0.0	0.0	6.9
T	11.5	15.8	65.4	0.0	69.2	0.0	2.3	5.0
CTRL	2.1	18.0	6.7	0.8	0.0	0.0	1.6	4.9

	Turbidimetry	NTA	SAXS							Cryo TEM
	τ (cm^{-1})	r_{NTA} (nm)	$\Delta\rho_a$ ($e^-.A^{-3}$)	r_a (nm)	r_b (nm)	r_c (nm)	n_b	n_{cCaP}	n_{cPl}	$\Gamma_{s/l}$
Full experimental design - 27 suspensions										
Average	21.2	61.0	0.015	45.6	10.7	1.6	3.3	171.5	318.9	8.5
SD	6.8	5.5	0.002	4.2	4.2	0.0	2.8	54.0	100.4	7.8
RSD (%)	32.1	9.0	13.5	9.3	38.9	3.1	84.1	31.5	31.5	91.0
minimum	12.6	53.8	0.010	41.5	6.1	1.5	0.2	75.3	140.0	0.9
maximum	43.8	74.8	0.018	58.1	21.9	1.7	13.3	243.7	453.3	35.6
Selected individual suspensions										
A	21.4	70.8	0.011	54.7	7.6	1.7	2.1	87.0	161.9	6.7
B	14.6	53.8	0.012	45.5	6.9	1.6	13.3	75.3	140.0	35.6
D	43.8	73.4	0.012	54.5	6.1	1.6	1.6	127.4	236.9	3.0
E	18.0	59.6	0.014	46.4	7.6	1.6	4.0	121.6	226.2	6.2
J	14.0	59.3	0.016	41.8	8.7	1.6	6.6	174.2	324.0	16.8
L	13.8	59.8	0.018	43.5	12.8	1.6	1.2	231.7	431.0	6.7
M	12.6	61.8	0.017	42.3	8.3	1.6	5.1	202.6	376.9	1.7
T	24.5	62.1	0.017	44.3	12.2	1.6	1.3	203.1	377.8	6.0
CTRL	15.7	57.0	0.018	41.5	10.1	1.5	4.0	228.0	424.1	4.6

	Firmness (A.U.)	RCT (min)
full experimental design - 27 suspensions		
Average	14.9	8.6
SD	5.1	9.8
RSD (%)	34.0	113.5
minimum	3.0	1.1
maximum	20.9	42.4
Selected individual suspensions		
A	3.3	1.4
B	11.5	2.9
D	14.0	1.4
E	16.2	2.9
J	8.0	24.6
L	17.5	11.2
M	3.0	42.4
T	20.9	3.4
CTRL	13.9	11.0

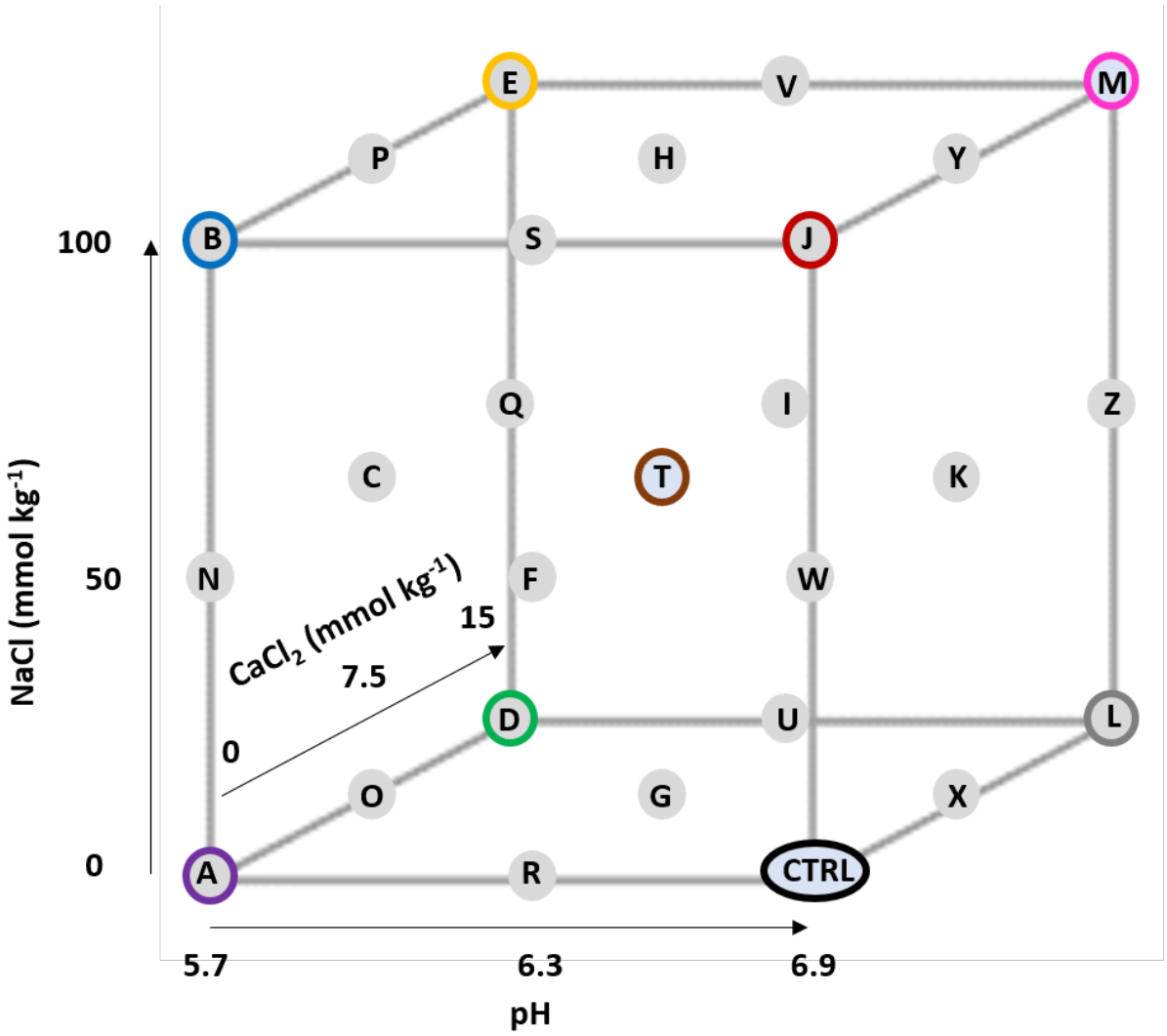
E
V
M
P
H
Y
100
B
S
J
Q
I
Z
C
T
K
50
N
F
W
15
7.5
0
D
U
L
O
G
X
0
A
R
CTRL
5.7
6.3
6.9
pH
NaCl (mmol kg-1)
CaCl2 (mmol kg-1)

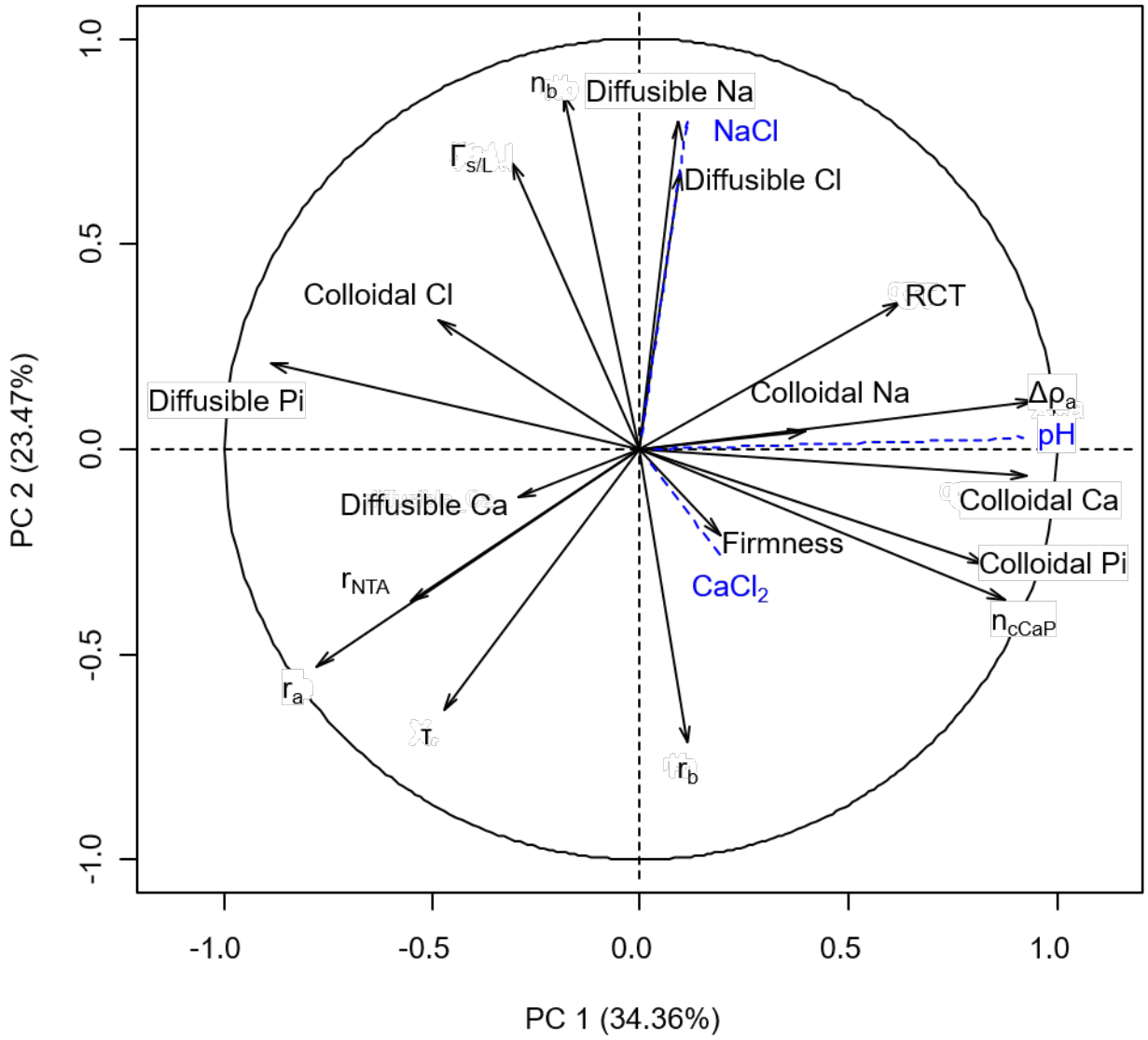
n_b
Diffusible Na
NaCl
$\Gamma_{s/L}$
Diffusible Cl
Colloidal Cl
RCT
Diffusible Pi
Colloidal Na
$\Delta\rho_a$
pH
Diffusible Ca
Colloidal Ca
Firmness
Colloidal Pi
r_{NTA}
$CaCl_2$
n_{cCaP}
r_a
τ_c
r_b
1.0
0.5
0.0
-0.5
-1.0
-1.0
-0.5
0.0
0.5
1.0
PC 2 (23.47%)
PC 1 (34.36%)

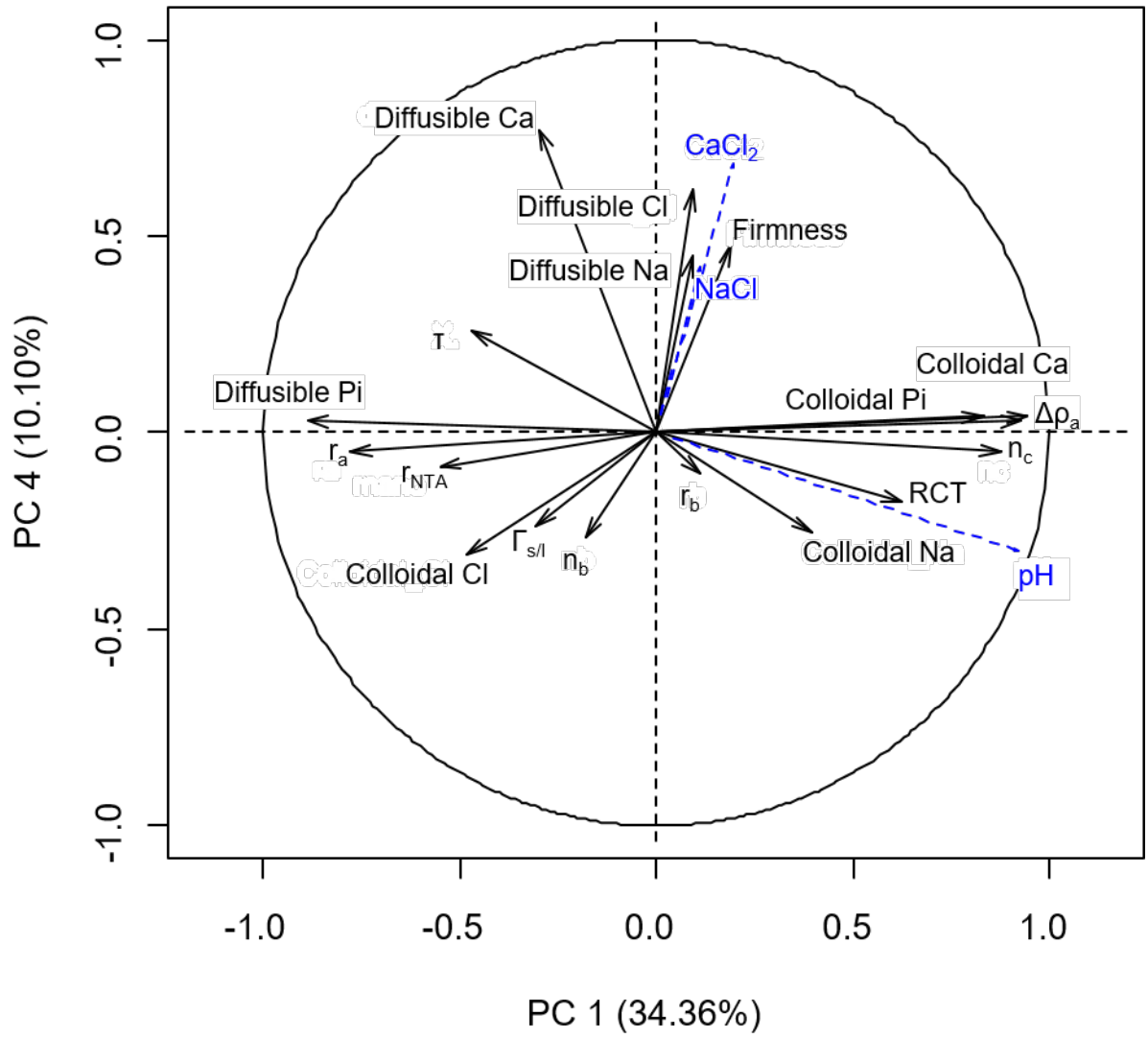
Diffusible Ca
CaCl2
Diffusible Cl
Firmness
Diffusible Na
NaCl
τ
Colloidal Ca
Diffusible Pi
Colloidal Pi
Δρa
ra
nc
rNTA
rb
RCT
Γs/l
nb
Colloidal Na
Colloidal Cl
pH
1.0
0.5
0.0
-0.5
-1.0
PC 4 (10.10%)
PC 1 (34.36%)

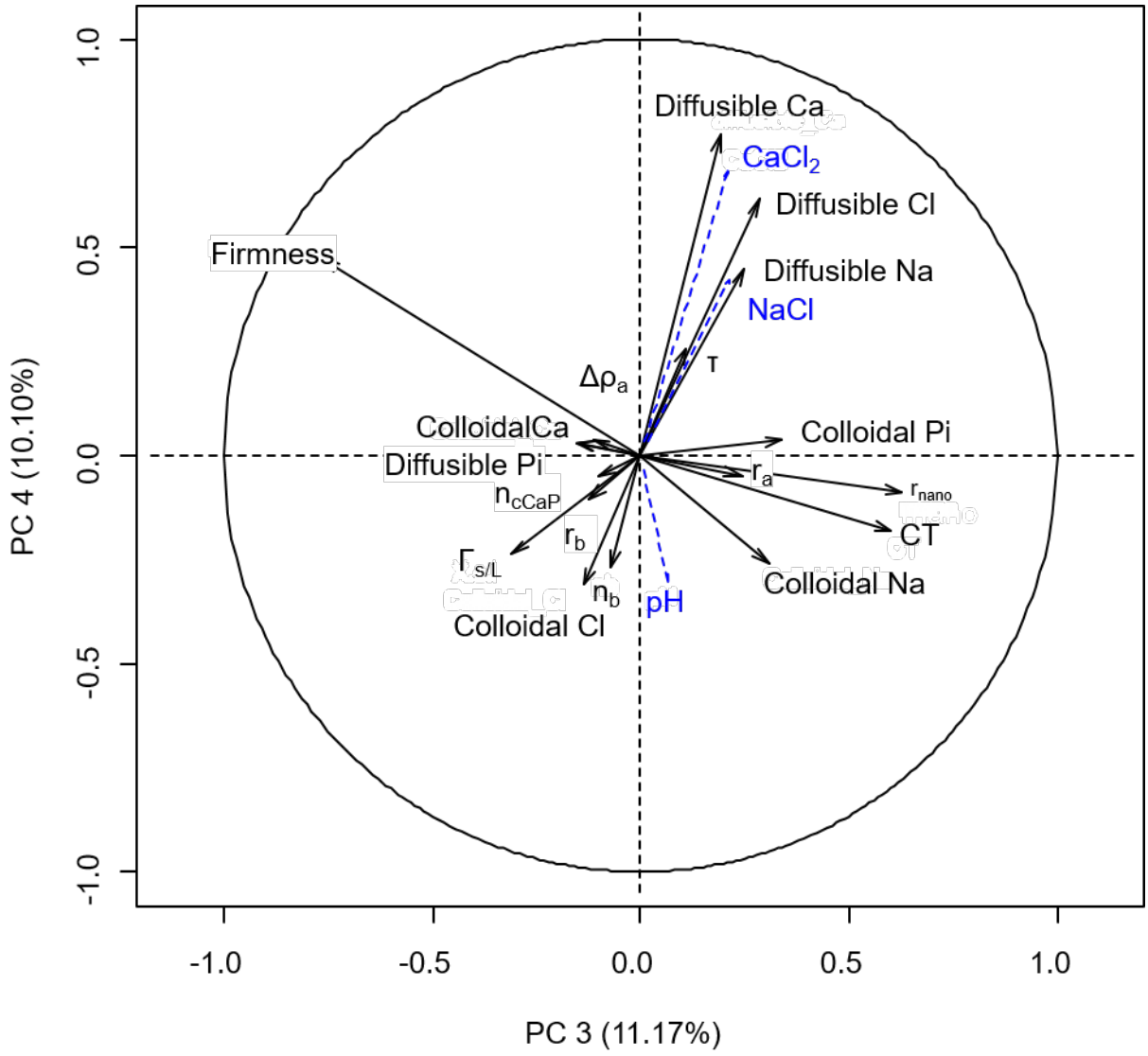
Diffusible Ca
CaCl2
Diffusible Cl
Firmness
Diffusible Na
NaCl
τ
Δρa
ColloidalCa
Colloidal Pi
Diffusible Pi
ra
rnano
nCCaP
CT
rb
Γs/L
nb
pH
Colloidal Na
Colloidal Cl
1.0
0.5
0.0
-0.5
-1.0
PC 4 (10.10%)
PC 3 (11.17%)

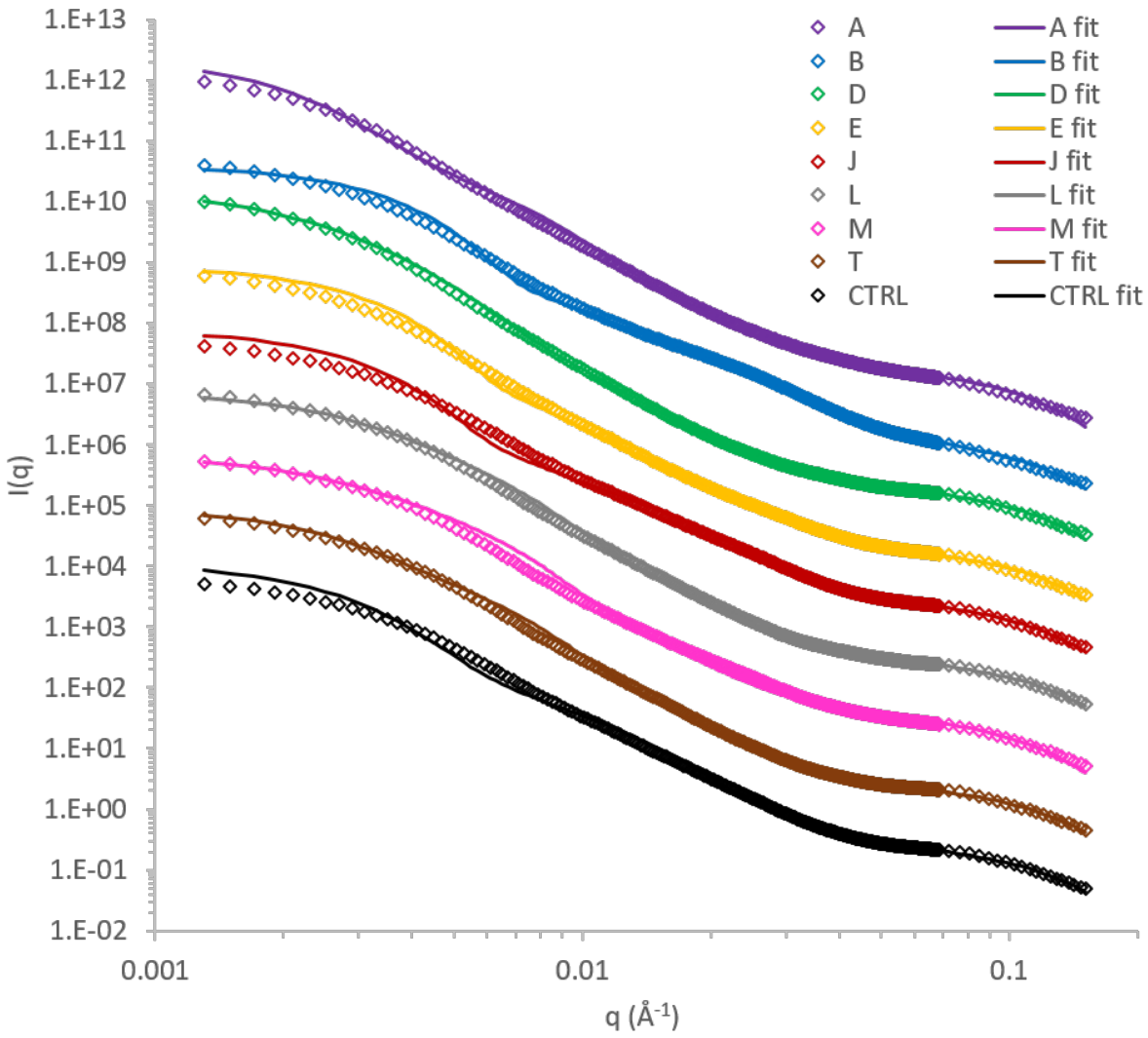
1.E+13
1.E+12
1.E+11
1.E+10
1.E+09
1.E+08
1.E+07
1.E+06
1.E+05
1.E+04
1.E+03
1.E+02
1.E+01
1.E+00
1.E-01
1.E-02
I(q)
0.001
0.01
0.1
q (Å-1)
A
B
D
E
J
L
M
T
CTRL
A fit
B fit
D fit
E fit
J fit
L fit
M fit
T fit
CTRL fit

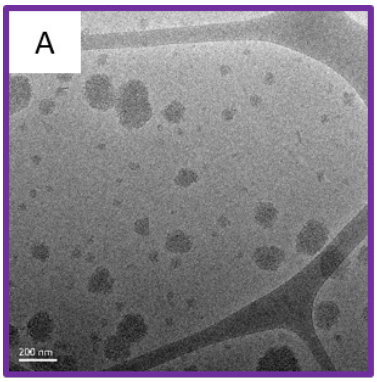
A
200 nm

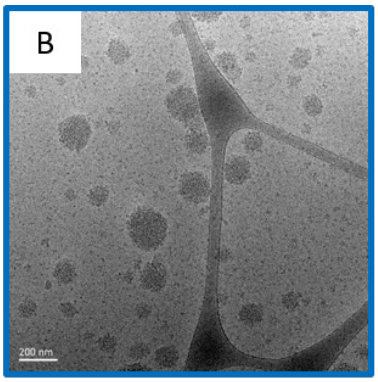
B
200 nm

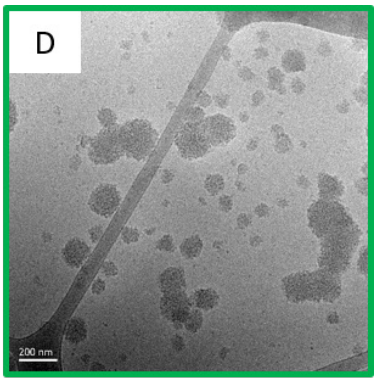
D
200 nm

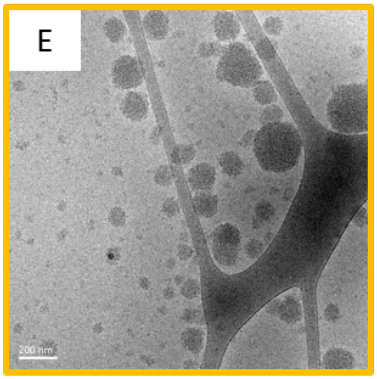
E
200 nm

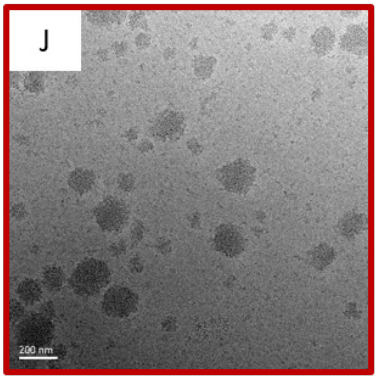
J
200 nm

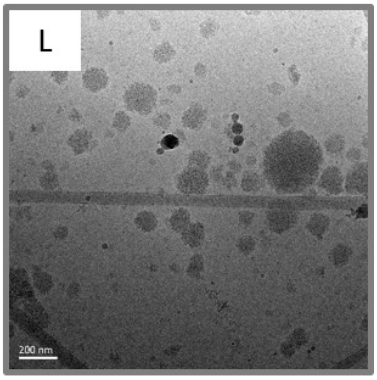
L
200 nm

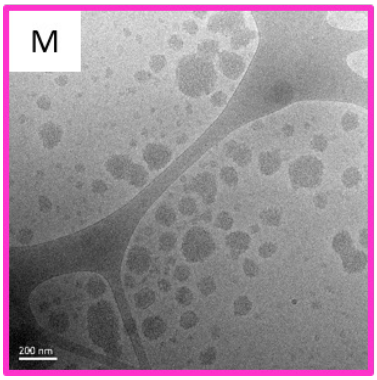
M
200 nm

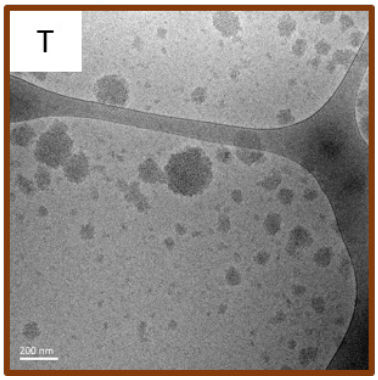
T
200 nm

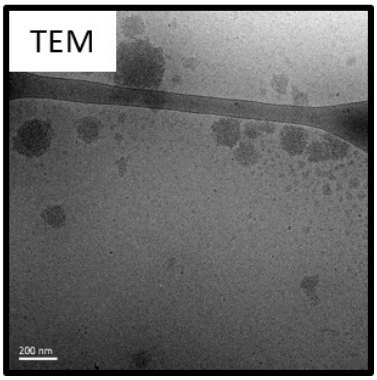
TEM
200 nm

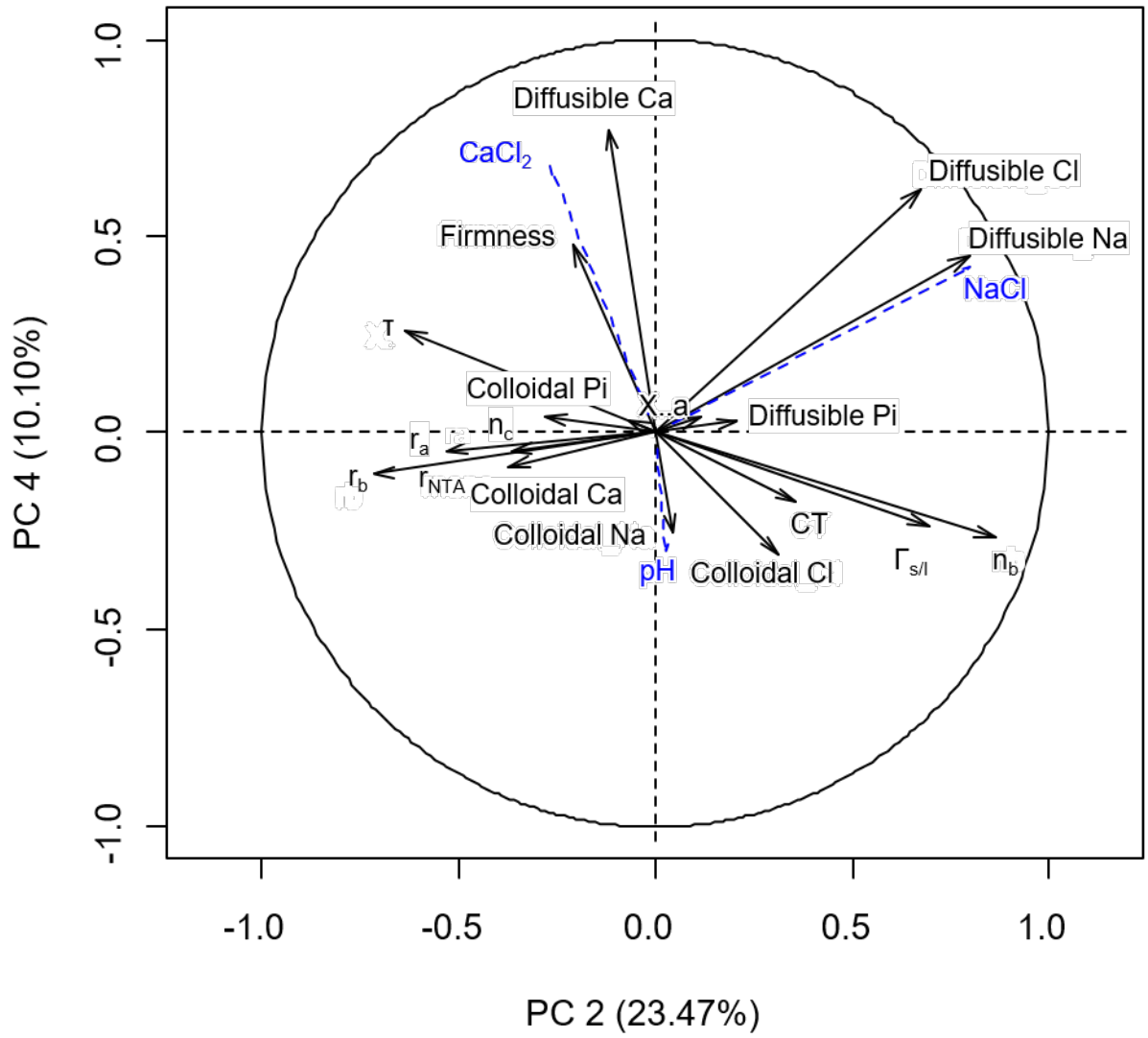
Diffusible Ca
CaCl2
Diffusible Cl
Firmness
Diffusible Na
NaCl
τ
Colloidal Pi
Diffusible Pi
nc
ra
rb
rNTA
Colloidal Ca
Colloidal Na
CT
pH
Colloidal Cl
Γs/l
nb
1.0
0.5
0.0
-0.5
-1.0
PC 4 (10.10%)
PC 2 (23.47%)

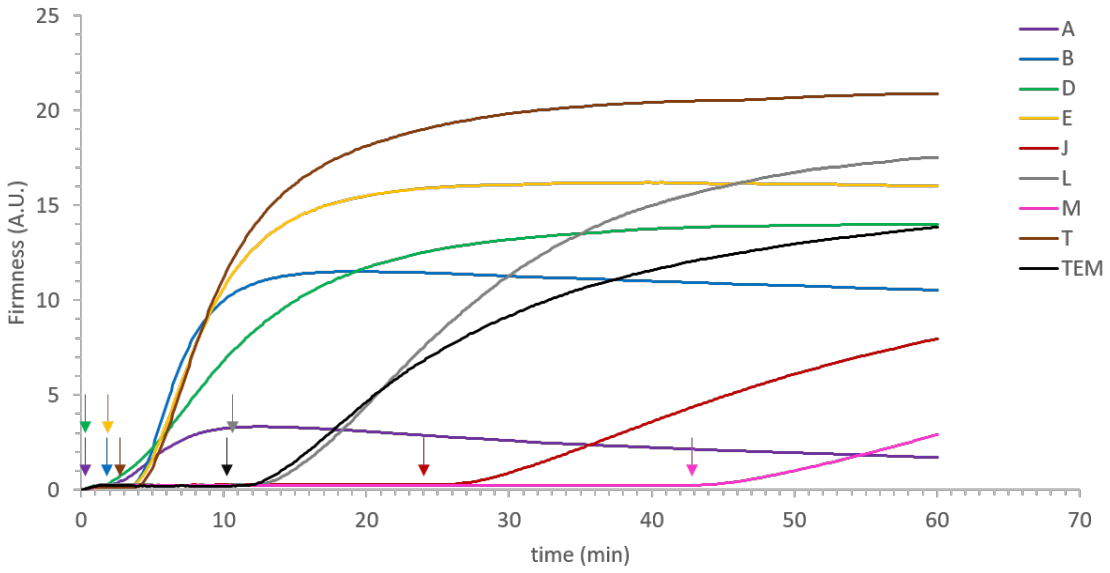
25
20
15
10
5
0
Firmness (A.U.)
0
10
20
30
40
50
60
70
time (min)
A
B
D
E
J
L
M
T
TEM

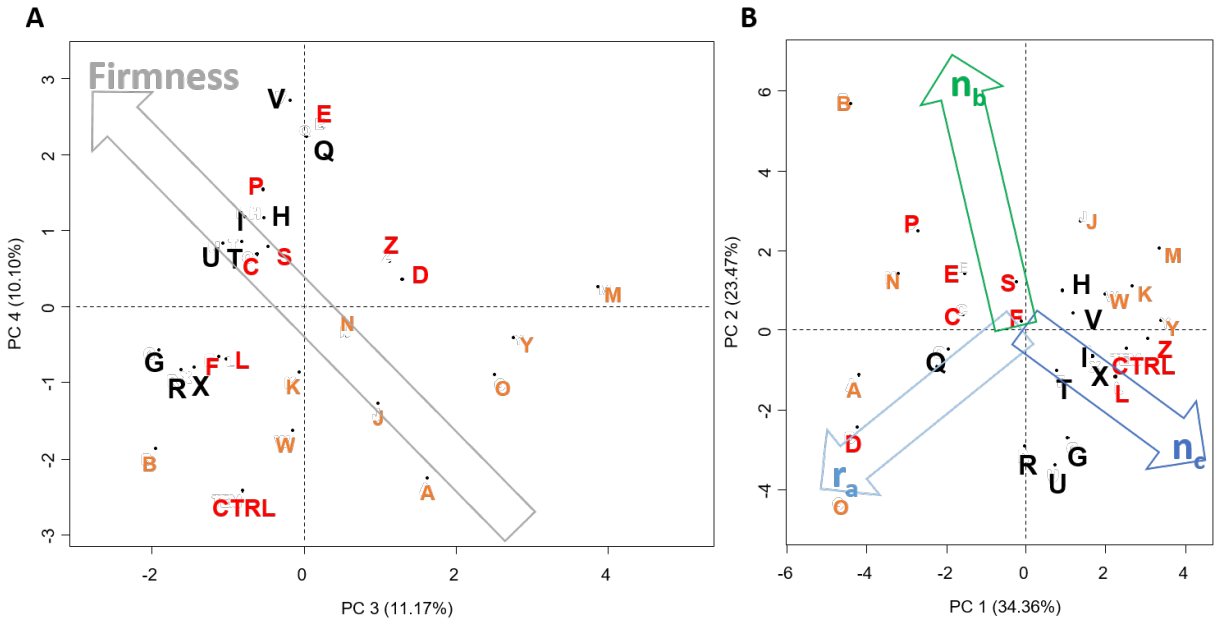
A
Firmness
PC 4 (10.10%)
PC 3 (11.17%)
B
PC 2 (23.47%)
PC 1 (34.36%)
CTRL

Author/s:
Lazzaro, F; Bouchoux, A; Raynes, J; Williams, R; Ong, L; Hanssen, E; Lechevalier, V; Pezennec, S; Cho, HJ; Logan, A; Gras, S; Gaucheron, F

Title:
Tailoring the structure of casein micelles through a multifactorial approach to manipulate rennet coagulation properties

Date:
2020-04-01

Citation:
Lazzaro, F., Bouchoux, A., Raynes, J., Williams, R., Ong, L., Hanssen, E., Lechevalier, V., Pezennec, S., Cho, H. J., Logan, A., Gras, S. & Gaucheron, F. (2020). Tailoring the structure of casein micelles through a multifactorial approach to manipulate rennet coagulation properties. Food Hydrocolloids, 101, https://doi.org/10.1016/j.foodhyd.2019.105414.